6-2011

Effects of Superhydrophobic Aerogel Surface Coatings on Drag Reduction

Robin A. Barabasz
Union College - Schenectady, NY

Effects of Superhydrophobic Aerogel Surface Coatings on Drag Reduction

By

Robin Barabasz

* * * * * * * * *

Submitted in partial fulfillment

of the requirements for

Honors in the Department of Mechanical Engineering

UNION COLLEGE

June, 2011

ABSTRACT

BARABASZ, ROBIN The Effects of Superhydrophobic Aerogel Surface Coatings on Drag Reduction. Department of Mechanical Engineering, June 2011.

ADVISOR: Ann Anderson, Ph.D.

The objective of this project was to determine if superhydrophobic aerogel-based surface coatings have an effect on hydrodynamic drag. Superhydrophobic aerogels were fabricated using Union College's patented rapid supercritical extraction technique. These aerogels were crushed and combined with a perfluorinated ion-exchange membrane to create a superhydrophobic coating that can be painted on to surfaces. These coatings are 250% aerogel by weight to Nafion in solution, and exhibit an average contact angle with water of 160°. An investigation of the aerogel powders and films using a scanning electron microscope (SEM) revealed that the most successful films had an average aerogel material width of 50 μm, uniform distribution of aerogel material on the coated slide, and that the peaks of the aerogel material coming into contact with the water had a feathery, crystalline appearance.

Three experiments were designed and conducted to determine if coating an object had an effect on the drag forces. The first experiment was a falling ball experiment, which examined the falling velocity of coated and uncoated balls gliding down an inclined surface. The second experiment used a rotational viscometer to examine the difference in torque required to rotate a spindle in water. The third experiment used particle image velocimetry (PIV) to examine the wake size of coated and uncoated cylinders in cross flow. For the conditions tested, no significant differences were

observed between coated and uncoated surfaces. These experiments were performed at low Reynolds numbers (between 613 and 10,258), which are characterized by a combination of friction drag and pressure drag. Future work with these surfaces should include testing in flows of higher Reynolds numbers, as well as conducting experiments that examine pressure drag and friction drag separately.

Table of Contents

Chapter 1: Introduction

Prior to the start of this project it was necessary to thoroughly research superhydrophobic surfaces. Below I will highlight the aspects of my research which correspond directly to the objectives of this project, as well as overview the work of Sarah Schinasi (Union College, 2010), whose senior project formed the foundations for this project.

Superhydrophobic Surfaces

Superhydrophobicity is a combination of hydrophobicity and micron-scale surface roughness. Hydrophobicity is most commonly quantified by the angle between the plane of the surface and the tangent to the surface of a droplet resting on it, known as the contact angle. Superhydrophobic surfaces exhibit high contact angles, beginning at 140° and approaching 180°. In some cases the beading of water droplets occurs due to the chemical composition of the surface which repels water and creates large interfacial tensions. In other cases the beading is caused by microscale surface roughness which prevents the water from wetting the entire surface, but rather causes drops to sit on the peaks of microposts. The hydrophobicity of a surface can also be expressed in terms of the slip length experienced by fluid elements near the surface. Superhydrophobic surfaces have achieved slip lengths on the order of 10 – 100 μm (Fugata et al., 2006). The micron-scale surface roughness can be measured using scanning electron microscope (SEM) images and atomic force microscopy (AFM).

Superhydrophobic surface fabrication can be characterized into top-down and bottom-up approaches. The top-down approach incorporates lithographic and template-based techniques, as well as plasma treatment of surfaces. The bottom-up approach involves self-assembly and self-organization of surfaces. Examples of the bottom-up approach include chemical deposition, layer-by-layer deposition, and hydrogen bonding (Li et al., 2007). For this project I will coat surfaces using a film incorporating superhydrophobic aerogels (which will be discussed in detail in a following section), but it is worth briefly acknowledging other methods.

In the case of microfluidics, ultrahydrophobic surfaces have been fabricated on silicon wafers using photolithography (Ou et al., 2004) and etching (Ma et al., 2006). These wafers have precise patterns of microposts and microridges that can be made hydrophobic through a chemical reaction with organosilane. "Nanoturf", a nanoengineered surface, is fabricated on silicon wafers using the black silicon method to create densely populated needle-like structures, 1 – 2 μm in height, across the surface of the wafer. The surface is then treated to be hydrophobic by spin coating of Teflon AF (DuPont) (Choi et al., 2006). Another way to apply a hydrophobic layer to a surface is through dip coating (Truesdell et al., 2006).

Drag Reduction by Superhydrophobic Surfaces

In any fluid flow, shear is caused by the difference between the free-stream velocity and the zero boundary velocity of the fluid particles due to the no-slip condition. The drag force experienced by an object in a fluid flow is the net force exerted by the fluid on the object in the direction of flow due to wall shear and pressure forces.

Although there are different types of drag, this project will focus specifically on drag in laminar flows. One way to reduce drag on an object in water is by making that object's surface superhydrophobic. The combination of microscale surface roughness and hydrophobic properties results in an air-water interface, supported by the surface tension of the water, trapping air between the microposts. This layer of air reduces the effective contact area between the fluid and the surface, as well as changes the macroscopic boundary condition on the surface from no slip to limited slip (Truesdell et al., 2006). The wall-shear stress is smaller with this streamwise slip, thus creating a reduction in drag (Min et al., 2004). Encouraging results have been gathered through experiments which quantify the drag reduction over superhydrophobic surfaces. A collection of the results from drag reduction experiments involving superhydrophobic surfaces can be found in Table 1.1.

A study of the kinematics of flows through microchannels using microparticle image velocimetry (μ-PIV) revealed that the maximum slip velocity occurred at the center of the shear-free air-water interface (Ou et al., 2005). This maximum slip velocity was more than 60% of the average velocity in the microchannel. It was also observed that the no-slip boundary condition existed along the surface of the hydrophobic microridges. The ultrahydrophobic surfaces used during this experiment were fabricated from silicon wafers using photolithography. The ridges were then made hydrophobic through a reaction with an organosilane.

Table 1.1: Collection of Drag Reduction Experiments; references in Appendix A

Reference	Flow Type	Testing Method	Surface Description	Results
[1]	1. Droplets over inclined surface 2. Laminar: Re=1500 and Re=11,000	1. Time for droplet to travel down inclined surface using a high speed camera 2. Hydrofoil in water tunnel; measured with force transducer	1. SH aerogel coated sandpaper (varying grit size) 2. SH coated textured surfaces, SH aerogel thin film process on smooth acrylic substrate (CA: 156°), non-coated smooth acrylic substrate	1. Drops on SH surfaces moved faster than non-SH. Optimum feature size determined to be ~8 μm; terminal velocity of 26 cm/s 2. At Re=1500, SH ~8 μm roughness had 18% drag reduction; at Re=11,000 it had only 7% drag reduction (see [1] for additional results)
[2]	Laminar and transitional (Re=370,000 – 407,000)	Water tunnel; measured with optical proximity sensor	Large-area nanograss surfaces; fabricated using photolithography, etching, and plasma vapor deposition	Drag reduction of 50% in laminar flow. As flow transitioned drag reduction decreased
[3]	Laminar	Microchannels; flow cell used to measure pressure drop as a function of flow rate	Ultrahydrophobic surfaces; fabricated from silicon wafers using photolithography, well defined micron-sized roughness, CA between 130° and 174°	Pressure drop reductions up to 40%, slip lengths of ~20 μm. No drag reduction observed for smooth hydrophobic surfaces
[4]	Laminar	Microchannels; flow cell used to measure the velocity profile and pressure drop as a function of flow rate, μ-PIV across microchannel	Ultrahydrophobic surfaces; fabricated from silicon wafers using photolithography, precise patterns of micrometer-sized ridges aligned in flow direction	Maximum slip velocity (~20 μm/s) of more than 60% the average velocity at the shear-free air-water interface, no-slip B.C. holds along surface of hydrophobic ridges
[5]	Laminar (Re =10 – 1000)	Cone-and-plate rheometer system	Nanoturf, hydrophobic by spin coating of Teflon, CA > 175°	Slip length of ~20 μm for water flow. Geometrical characteristics of nanoposts are significant
[6]	Laminar (low Re)	Couette cell; measured with a strain-controlled rheometer, PIV	PDMS substrates dip-coated in SH aerogel solution, patterned 25-μm grooves, applied with double-sided adhesive tape	Macroscopic slip caused a drag reduction of approximately 20%
[7]	Laminar ($Re=10^4 \sim 2x10^4$) and turbulent ($Re=2x10^6 \sim 5x10^6$)	Rotaty flume (laminar) and water tunnel (turbulent)	Nano-alumina structures modified by flouro-coatings	At low Re, drag reduction of 8.76%. Friction increased under turbulent flow
[8]	Laminar	Microchannels; measured flow rates at various pressure differences with flow metering system	Silicon wafers were etched and chemically treated	Slip length varied linearly with the shear rate; 30 nm at a shear rate of $10^5\ s^{-1}$
[9]	Laminar and turbulent	Rotating disk	Coated with water-repellant material; CA 120°	45% drag reduction at $Re=10^5$ in aqueous of glycerin of 40 wt%

***Note: This does not include mathematical and computer simulations of experiments**

Another similar study with ultrahydrophobic surfaces produced pressure drop reductions up to 40% and apparent slip lengths larger than 20 μm (Ou et al., 2004). These surfaces were also fabricated from silicon wafers using photolithography. A flow cell was used to measure the pressure drop as a function of flow rate for a series of microchannel geometries and ultrahydrophobic surface designs. The deflection of the air-water interface was measured using a confocal surface metrology system.

Large-area test surfaces have also been analyzed. In one particular study (Henoch et al., 2006), a water tunnel was used to measure drag in both laminar and transitional flows at velocities up to 1.4 m/s. In the laminar flow, a drag reduction of approximately 50% was observed. At higher speeds, after the flow transitioned to turbulence, lower levels of drag reduction were observed. The large-area test surfaces were fabricated from silicon wafers using photolithography and deep reactive ion etching.

One especially interesting method (Gogte et al., 2005) used a high-speed digital video camera to measure the speed at which a water drop rolls down an inclined (1° to 3°) superhydrophobic surface. The superhydrophobic surfaces were fabricated using aerogels to coat sandpaper of various grit sizes. The highest drop velocities occurred on surfaces with irregular textures with characteristics feature size of approximately 8 μm. When the same texture and coating was applied to the surface of a hydrofoil in a water tunnel, a drag reduction of 10% was observed.

Aerogels

Aerogels are a class of ceramic materials. They have a porous nanostructure that is approximately 90 – 99% air by volume, with high surface area, low density, low thermal and electrical conductivity, and visible transparency. Aerogels are made from a basic two-step procedure. The first step is the formation of a wet gel through a sol-gel polymerization reaction of precursor chemicals. The second step is the extraction of the sol-gel solvent, which leaves a dry, rigid nanostructure behind. Silica aerogels are hydrophilic, but techniques exist to make aerogels hydrophobic by replacing the hydrophilic hydroxyl groups through surface modification (Anderson et al., 2009).

The transportation of water droplets on a superhydrophobic silica aerogel-powder-coated surface was studied by Rao et al. in 2005. A device was used to measure the velocity of water drops down an inclined surface coated with superhydrophobic aerogel powder. The microstructure of the aerogel had an effect on both the shape of the water droplet and the velocity of the water droplet. Water drops on an aerogel powder with uniform, small particle size had a maximum velocity of 144 and 123 cm/s, while water drops on an aerogel powder with non-uniform, bigger particle size had a minimum velocity of 92 and 82 cm/s. The aerogels used in the experiment were fabricated by supercritical drying using methanol solvent.

Superhydrophobic surfaces have been fabricated using aerogels. A study of the effective slip on textured superhydrophobic surfaces by Gogte et al. in 2005 uses aerogels to coat sandpaper. Sandpaper of various grit size was dip coated in the precursor chemical mixture, then the aerogel was fabricated through a low temperature/pressure

thin film process. This coating, applied to a smooth acrylic substrate, had an average contact angle with water of 156°.

Prior Work by Sarah Schinasi (Union College, 2010)

This project is a continuation of Sarah Schinasi's senior project, *The Effects of Surface Finish on Drag: Coatings of Racing Shells* (Schinasi, 2010). The purpose of her project was to design a lightweight surface coating for racing shells that reduces the drag due to surface friction. Overall her results supported the theory that superhydrophobic surfaces reduce drag. She was able to successfully fabricate a superhydrophobic film by adding superhydrophobic aerogel powder to Nafion, a sulfonated tetraflouroethylene based fluoropolymer-copolymer manufactured by DuPont. The recipe of the final film contained 1.4995 grams of powdered superhydrophobic aerogel, 13 ml of Nafion, and 1.25 ml of propanol. When painted on a test surface this film exhibited a contact angle with water of 162°. A dynamometer was used to measure the drag on test pieces placed in a circulating water tank (Andy Krauss, 2008). At velocities of about 0.8 m/s, the drag on the superhydrophobic test piece was approximately 0.125 N, while the drag on the uncoated piece was 0.138 N. At Reynolds numbers around 140,000, the superhydrophobic test piece had a drag coefficient of about 0.028 compared to 0.031 for the uncoated test piece. However, the irregularity of the flow within the water tank caused high standard deviation in her data, so further studies are required to confirm the effect.

The remainder of this report summarizes the film fabrication process, as well as the results from three experiments. Chapter 2 details the superhydrophobic aerogel surface fabrication process, as well as challenges I encountered while making quality superhydrophobic films. Chapter 3 details a falling ball experiment that examined the velocity of coated and uncoated balls gliding down an inclined surface. Chapter 4 details an experiment that used a rotational viscometer to measure the torque required to rotate coated and uncoated spindles in water. Chapter 5 details an experiment that used particle image velocimetry to examine the wake of coated and uncoated cylinder in cross flow. The attached appendices contain pictures, procedures, raw data, and other additional materials.

Chapter 2: Superhydrophobic Aerogel Surface Fabrication

The contents of this chapter relate to superhydrophobic aerogel surface fabrication. I successfully fabricated superhydrophobic aerogels using the rapid supercritical extraction process. A technique was developed to crush these aerogels into a uniform powder. These powders were then combined with Nafion and propanol to make superhydrophobic films. Scanning electron microscopy and nitrogen gas adsorption were used to characterize the powders and films. Included in this chapter are challenges I faced during the surface fabrication process, as well as the main conclusions that can be drawn from this process.

Aerogel Fabrication

Superhydrophobic aerogels were fabricated using Union College's patented rapid supercritical extraction process. The superhydrophobic aerogels were 50:50 tetramethoxysilane (TMOS) to methyltrimethoxysilane (MTMS) by volume. Table 2.1 summarizes the batches of aerogels that were made, including dates of fabrication and details about the fabrication process.

Table 2.1: Summary of aerogel fabrication

Batch	Date of Fabrication	Recipe	Mold	Hot Press Program
RB2	6/25/2010	150 ml	B	2A
RB3	7/30/2010	60 ml	A	2A
RB4	9/23/2010	60 ml	A	2A
RB5	9/30/2010	60 ml	A	2A
RB6	10/7/2010	150 ml	B	2A
RB7	11/8/2010	150 ml	B	2B
RB8	1/11/2011	150 ml	B	2B

The recipes, hot press programs, pictures of molds, and pictures of aerogels can be found in Appendix B. The main difference between the aerogels was due to the hot press program used during fabrication. Program 2A pre-gelled for three hours in the beginning of the fabrication process, while program 2B did not pre-gel. This made the aerogels visibly different, and also affected the quality of the films fabricated with the aerogels. This will be discussed in depth in a later section.

Quantifying Hydrophobicity

The hydrophobicity of the aerogels, as well as the powders and coated slides (to be discussed later), was measured using a Kruss Drop Shape Analyzer (DSA 100). Using this instrument, water of specified drop size can be placed onto a surface using a precision needle (shown in Figure 2.1).

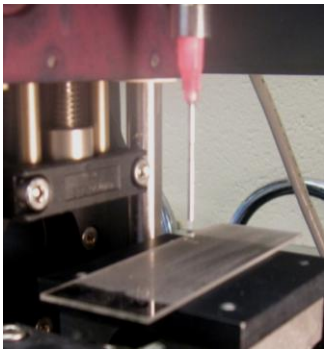

Figure 2.1: Kruss Drop Shape Analyzer

A computer software program, DSA3, was then used to measure the contact angle based a picture of the water drop taken by a camera in the instrument. The contact angle was estimated using Young-Laplace sessile drop fitting. Figure 2.2 shows an image taken of two drops of water placed on a coated slide. One drop is on a hydrophobic region, while

the other is on a hydrophilic region. This illustrates the non-uniformity of the preliminary films.

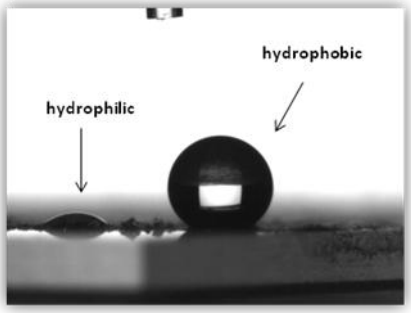

Figure 2.2: Image taken with Kruss Drop Shape Analyzer;
contact angle of 158° on the hydrophobic region

Aerogel Powders

Once superhydrophobic aerogels were fabricated, the next step was determining a method to crush the monoliths into a powder of uniform particle size. A variety of crushing techniques were explored. Pictures regarding crushing methods, as well as pictures of powders can be found in Appendix C. The most successful method was determined to be crushing the aerogels by hand for 20 minutes with a mortar and pestle, using propanol as a solvent. To confirm that using propanol as a solvent did not decrease the hydrophobicity of the aerogel, double-sided tape was used to capture the powder for contact angle measurements (Figure 2.3).

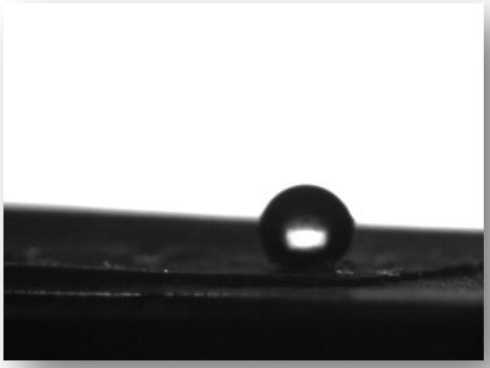

Figure 2.3: Drop of water on double-sided tape covered with superhydrophobic aerogel powder; contact angle of 177.3°

Most of the powders were so hydrophobic that drops of water could not even be placed on the tape. Once it was determined that better powders were obtained crushing with propanol (which would evaporate from the aerogel material by drying overnight in the hood), experiments with different crushing times (5, 15, and 30 minutes) were performed. There were no visible differences between the powders crushed for 15 and 30 minutes, so from that point on the powders were crushed for 20 minutes. Crushing by hand was time consuming, and only a small amount of aerogel could be crushed at a time. Techniques were explored that would allow more material to be crushed at once, and would also guarantee a uniform particle size of aerogel material. The best available option was a ball mill. The ball mill was used by placing a plastic nalgene bottle, filled with aerogel and zirconia grinding media, on the rollers, and rolling for a specified amount of time at a specified speed. Different amounts of aerogel material, as well as crushing dry versus wet (using propanol) were examined during trial experiments. Grinding wet was not successful; the aerogel material clumped together and stuck in a solid mass with the grinding media. Grinding dry, however, worked quite well. The powdered aerogel could easily be separated from the grinding media using a sifter. This method did not require

that the powder be dried after crushing. It also guaranteed that anyone following the procedure for crushing the aerogels would create a powder of the same particle size and uniformity. Unfortunately, the films made from the aerogels powdered using the ball mill were not as hydrophobic as past powders crushed by hand. This was believed to be due to the aerogels themselves, not the grinding technique. For the sake of completeness the results are summarized in the tables below.

Table 2.2: RB3 aerogels – powdered on the ball mill for 10 minutes, final film recipe, double coat

Contact Angle Measurements		
	Slide A	Slide B
average	136°	138°
st. dev	11°	13°
% st. dev	8%	9%

Table 2.3: RB3 aerogels – powdered on the ball mill for 10 minutes, 500 wt % aerogel to Nafion

Contact Angle Measurements	
average	122°
st. dev	9°
% st. dev	7%

Table 2.4: RB4 aerogels – shaking technique (20x), final film recipe

Contact Angle Measurements	
average	122°
st. dev	6°
% st. dev	5%

The surface area and pore distribution of the aerogels was measured using both a Micrometrics TriStar Gas Adsorption System and an Accelerated Surface Area and

Porosimetry Analyzer. Samples were degassed for 1 -2 hours at 90 °C, then 4 – 6 hours at 200 °C before testing. The results from the BET surface area test are shown in Table 2.5.

Table 2.5: BET surface area

Sample	Surface Area (m^2/g)
RB2	801
RB2 – powder	801
RB4	939
RB5	967
RB6	943

The results from the BJH pore distribution are shown in Figure 2.4.

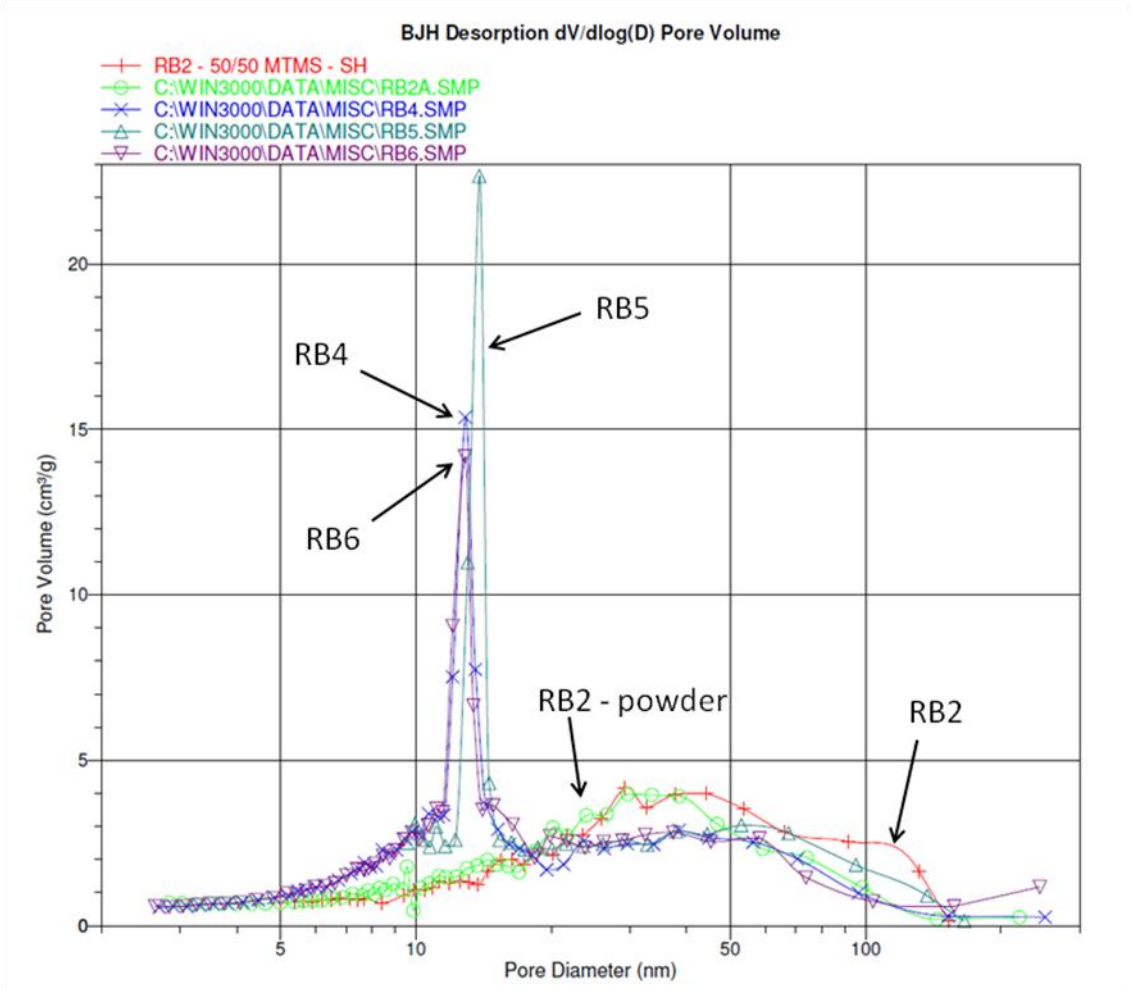

Figure 2.4: BJH pore distribution

The surface area of RB2 was less than that of the other batches (although still quite high). The pore distribution was also different. RB2 had no characteristic peak in pore diameter, while the other batches had large peaks around 15 nanometers. This was believed to be due to the way the aerogels were fabricated.

The microscopic characteristics of some of the aerogel powders were examined using a Zeiss EVO50 Scanning Electron Microscope (SEM). The objective of using the SEM was to determine if there was a visible difference between aerogel powders that made successful (very hydrophobic) and unsuccessful (slightly hydrophobic) films. The powders from batches RB2 and RB5 (these films will be discussed in a later section). Figure 2.5 is an image of RB2 powder, while Figure 2.6 is an image of RB5 powder.

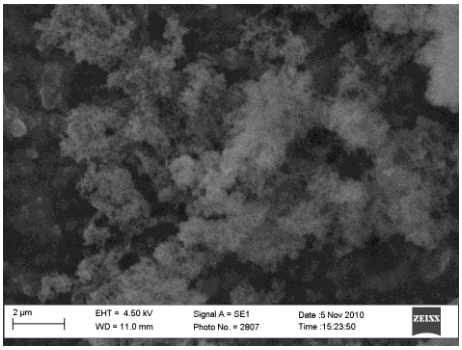

Figure 2.5: SEM image of RB2 powder (courtesy of Mark Hooker)

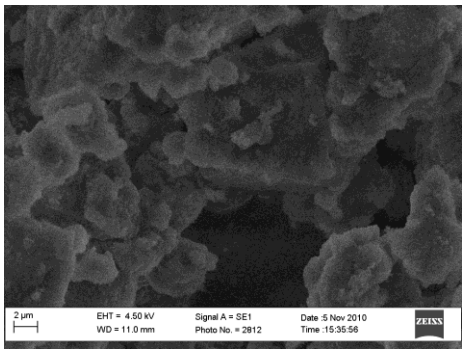

Figure 2.6: SEM image of RB5 powder (courtesy of Mark Hooker)

These powders are quite different. The RB2 powder has a feathery, crystalline appearance, while the RB5 powder appears to be an ordered amorphous solid. The differences were attributed to the fabrication process; RB5 was pre-gelled while RB2 was not. The way these powders affect the hydrophobicity of the films will be discussed in a later section.

Aerogel Films

The first challenge in fabricating superhydrophobic films was determining the optimal loading of aerogel by weight to Nafion in solution. Two series of six preliminary films were prepared on glass microscope slides. For each powder (5, 15, and 30 minutes), 10% and 50% aerogel by weight was added to 2 ml of Nafion. One set of films was dried rapidly in an open hood (Appendix D), while the other set was placed in a closed tupperware container to dry slowly (Appendix F). Contact angle measurements were taken to see if the properties of the hydrophobic aerogel were retained on the slides (Appendix E). These films were not hydrophobic. Certain regions on the slides exhibited hydrophobic properties while others were entirely hydrophilic. A film with 5% aerogel by weight to Nafion was also fabricated (Appendix G), and as expected, this film was not hydrophobic.

A series of control experiments were performed to indicate whether outside factors were affecting the quality of the films. To eliminate the possibility of a coating on the slides, although the packaging specified they were pre-cleaned, the slides were

prepped by dipping them in propanol. From that point on, every slide was rinsed with propanol before use.

The preliminary films were not hydrophobic, therefore a series of films was fabricated with much higher concentrations of aerogel. Films were fabricated with solutions of 75, 100, and 125% aerogel (powdered for 30 minutes) by weight added to 2 ml of Nafion. These solutions were poured onto slides and dried open in the hood. These films were all fairly uniform; the aerogel particles formed into clusters and there was minimal cracking (Appendix H). Some regions of these films were hydrophobic while others were not. This was believed to be due to the fact that the water drops used to measure contact angle were too large to rest on the clusters of aerogel material, and spread out once they came in contact with the slide.

Sarah Schinasi's final film was approximately 250% aerogel by weight to Nafion. This film was replicated to test the concentration. The recipe included 2 ml of Nafion, 2 ml of propanol, and 250% aerogel (crushed for 30 minutes). A paintbrush was used to apply the solution onto slides (single coat and double coat). These slides were hydrophobic. The slide with the single coat had an average contact angle of 161° (see Appendix I). These films were the most hydrophobic that had been fabricated (to date), therefore it was determined that the optimal loading was 250% aerogel by weight to Nafion.

Once the optimal concentration of aerogel by weight to Nafion was determined, films were made using two additional solutions of Nafion. The original Nafion solution (used by Sarah Schinasi) was 5 wt.% polymer content, 45 wt.% water, and 50 wt.% alcohol (propanol). Solutions of 20 wt.% polymer content, 20 wt.% water, and 60 wt.%

alcohol (propanol), and 5 wt.% polymer content, 15 – 20 wt. % water, and 75 wt.% alcohol (propanol) were purchased from Sigma-Aldrich. Three solutions were made, each 250% superhydrophobic aerogel (20 minutes crushed with propanol) by weight respective to the Nafion used (Table 2.6) (see Appendix J).

Table 2.6: Recipes for films with different Nafion solutions

Film 1	**Film 2**	**Film 3**
(5 wt.% Nafion, 45 wt.% water)	(20 wt.% Nafion, 20 wt.% water)	(5 wt.% Nafion, 15 – 20 wt.% water)
2 ml Nafion	2 ml Nafion	2 ml Nafion
0.231 g RB2 aerogel	0.976 g RB2 aerogel	0.218 g RB2 aerogel
4 ml propanol	12 ml propanol	4 ml propanol

The hydrophobicity of these films was quantified by taking contact angle measurements and calculating the average contact and angle and standard deviation (Table 2.7).

Table 2.7: Contact angles of Nafion films

	Film 1	**Film 2**	**Film 3**
average	150°	151°	160°
std dev	14°	18°	7°
% std dev	9%	12%	4%

The films were also tested for degradation in water. A coated slide of each film was soaked in a beaker of tap water for approximately 16 hours. As predicted, the average contact angle for each of the films decreased (Table 2.8).

Table 2.8: Contact angles of Nafion films after soaking in water

	Film 1	**Film 2**	**Film 3**
average	137°	126°	143°
std dev	8°	11°	5°
% std dev	6%	8%	4%

It was concluded that Film 3 was the most successful coating fabricated. It exhibited the highest contact angle with water, was most hydrophobic after prolonged exposure to water, and was the most uniform. Appendix K lists the procedure of the final film fabrication.

During the film fabrication process, it became apparent that certain batches of aerogels were producing films of higher hydrophobicity than others. A direct comparison of each batch was performed by replicating the exact final film. The results are summarized below.

Table 2.9: RB4 aerogels – exact final film replication

Contact Angle Measurements		
	Slide A	Slide B
average	114°	112°
st. dev	7°	5°
% st. dev	6%	4%

Table 2.10: RB5 aerogels – exact final film replication

Contact Angle Measurements		
	Slide A	Slide B
average	131°	129°
st. dev	6°	6°
% st. dev	4%	5%

Table 2.11: RB2 aerogels – exact final film replication

Contact Angle Measurements		
	Slide A	Slide B
average	153°	157°
st. dev	10°	8°
% st. dev	7%	5%

Surprisingly, the only film that could successfully replicate the final film used aerogels from batch RB2. It was hypothesized that batch RB2 had some physical property that was

different than the other batches. The majority of the first term of this project was dedicated to trying to determine what that difference was, what caused the difference to occur, and most importantly, how batch RB2 could be replicated. RB2 was an outlier; even visibly it was quite different than the other batches (see Appendix B). The aerogels from RB2 were white, while the aerogels from all other batches (batches RB3, RB4, and RB5) were slightly transparent and lighter in color. All the batches were made using the same recipe (although the volumes differed according to the mold used) and the same hot press program, although RB2 was made using a different mold. Batch RB6 was fabricated using the mold used to make RB2, but still the films were not hydrophobic (see results in Table 2.12).

Table 2.12: RB6 aerogels – exact final film replication

Contact Angle Measurements		
	Slide A	Slide B
average	117°	133°
st. dev	9°	21°
% st. dev	8%	16%

Although we could hypothesize about how to interpret the surface area and pore distribution results (Table 2.5 and Figure 2.4) based on the hydrophobicity of the films, we couldn't make any concrete conclusions. Professor Anderson suggested I look at superhydrophobic aerogels made by Emily Green during her summer research in 2007. One batch of her aerogels, EG - 8, had a similar pore distribution to RB2. One of her samples was used to make a film (see Appendix L for results). This film was hydrophobic. Some areas of the slides were so hydrophobic that drops could not even be placed on the surface. The only other films exhibiting this behavior were made using aerogels from batch RB2. This led to an examination of the recipe and the hot press

program used to fabricate EG – 8 (Appendix L). The recipe was the same as the recipe used to fabricate my aerogels, however EG – 8 had twice the amount of catalyst. The hot press program was also different; EG – 8 was not pre-gelled during the fabrication process. The program I had been using pre-gelled for 3 hours during the first step of the hot press program. This information about EG – 8 was related to batch RB2. RB2 was fabricated during the beginning of summer research, when the catalyst used could have been weak (usually a new batch of catalyst is made at the beginning of each semester). If the catalyst was weak, it would have had a similar effect on RB2 as not pre-gelling. This would have made the fabrication process similar to EG – 8, and dissimilar to the other batches of aerogels that were made. Batch RB7 was made without pre-gelling (hot press program in Appendix B) in the same mold used with batch RB2. This was done in an effort to replicate the exact conditions under which batch RB2 was fabricated. The fabrication of RB7 did, in fact, successfully replicate RB2. The aerogels were visibly identical to those from batch RB2, and made a film that was very hydrophobic (so hydrophobic that drops could not be placed on the surface). Determining how to successfully replicate batch RB2 was crucial to the success of this project. It was learned that simply using superhydrophobic aerogels was not enough to fabricate quality superhydrophobic films. Theories were generated about why aerogels that are not pre-gelled during the fabrication process produce films that are more hydrophobic than those made with aerogels that are pre-gelled, but nothing can be confirmed about what the true cause is without further investigation. It may be due to the differences in the formation of the crystalline nanostructure, which occurs during different stages of the fabrication

process based on whether the aerogels are pre-gelled or not pre-gelled. An examination using the SEM led to the belief that the difference lies in the crystalline structure.

The microscopic characteristics of the films were examined using the scanning electron microscope (SEM). The objective of using the SEM was to determine if there was a visible difference between successful and unsuccessful films. Films made using aerogels from batches RB2 and RB5 (as well as the aerogel powders used to make the films, mentioned earlier) were examiend. As predicted, both the powders and the films were very different. Figure 2.7 is an image of a film made with RB2 aerogels, while Figure 2.8 is an image of a film made with RB5 aerogels; these images were taken at a similar magnification.

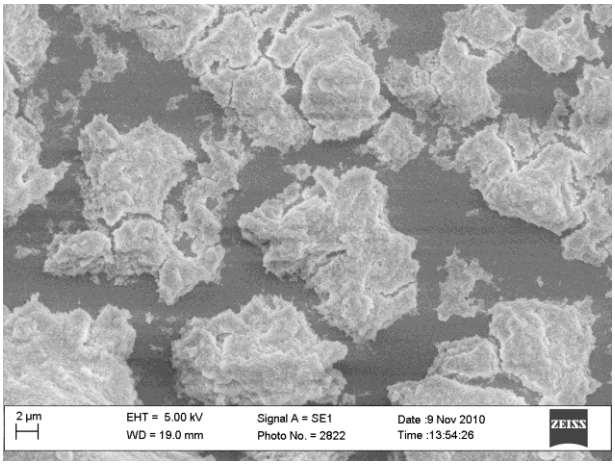

Figure 2.7: SEM image of film made with RB2 aerogels (courtesy of Mark Hooker)

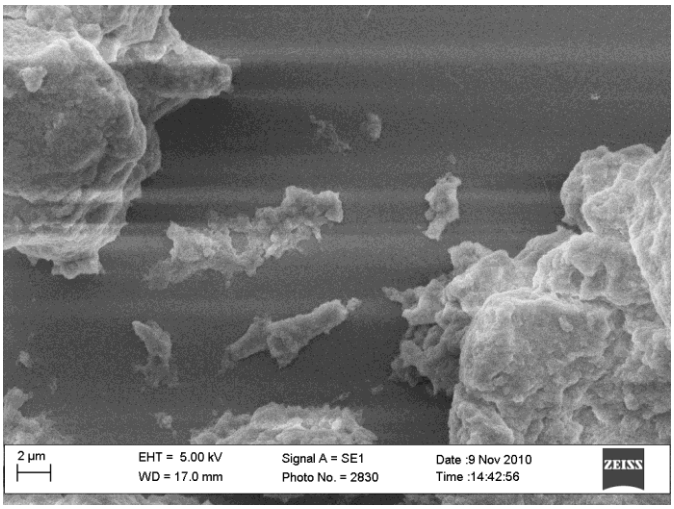

Figure 2.8: SEM image of film made with RB5 aerogels (courtesy of Mark Hooker)

Notice the difference in the size of the aerogel material. Prior to examining the slides with the SEM, it was unknown how the aerogel material was combining with the Nafion on the slides. The images show that the aerogel material clumps together, rather than remaining as the particles in the powder. It is believed that the RB2 film is more hydrophobic than the RB5 film due to the size of the clusters of aerogel material, the distribution of the material (the space between the clusters of material), and the crystalline structure at the peaks of the aerogel material that is in contact with the water. Figure 2.9 shows an image of the two coated slides next to each other, which allows them to be compared directly under the same magnification.

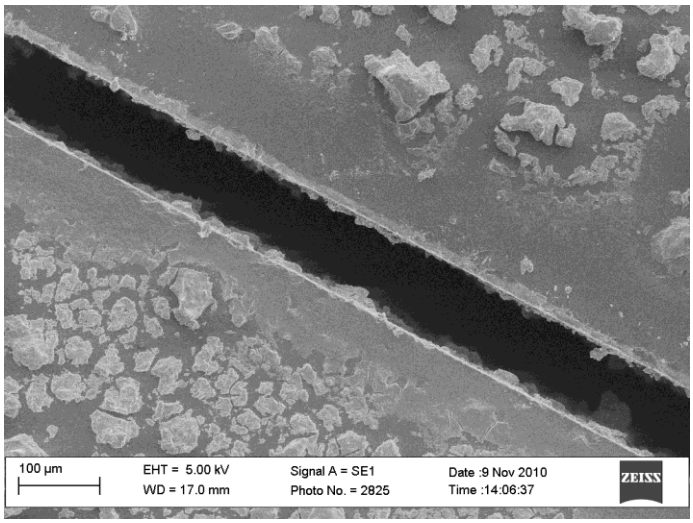

Figure 2.9: SEM image of films RB2 (bottom) and RB5 (top) (courtesy of Mark Hooker)

The aerogel material in the RB2 film formed into smaller clusters and was distributed uniformly across the slide. The aerogel material in the RB5 film formed into large clusters and was non-uniformly distributed. Figure 2.10 is a larger view comparing slides coated with RB2 and RB5 film.

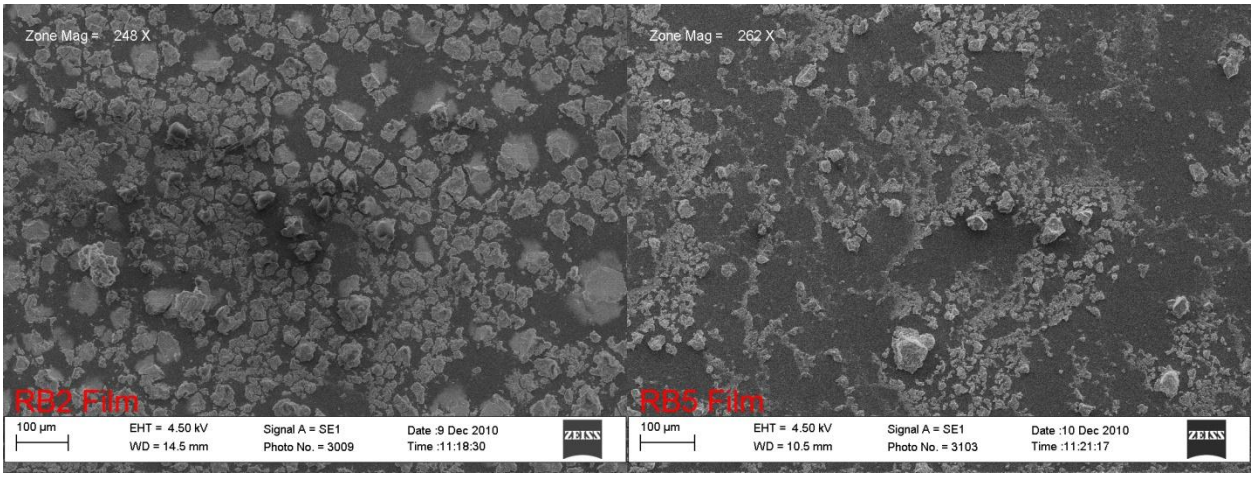

Figure 2.10: SEM images of RB2 (left) and RB5 (right) films (courtesy of Nick Dunn)

It is also worth noting the size of the aerogel clusters and the space between clusters. Figure 2.11 shows an area of the RB2 film that is representative of the coating on the entire slide.

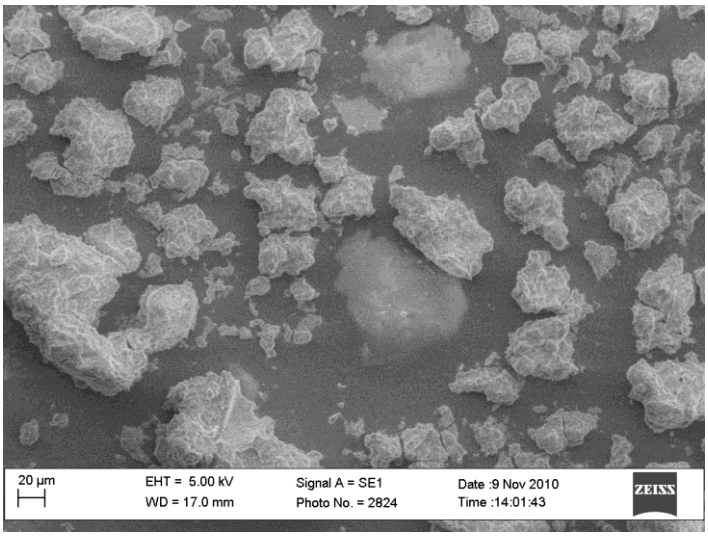

Figure 2.11: SEM image of film made with RB2 aerogels (courtesy of Mark Hooker)

The average width of the aerogel clusters is 50 µm. The material is uniformly distributed, with only small gaps between the aerogel clusters. This surface texture was then compared to information published about man-made superhydrophobic surfaces. One article was particularly helpful with making sense of the results; "For microposts between 10 µm to 40 µm across, contact angle is nearly independent of cross sectional geometry, post height, and surface chemistry. However, a significant deterioration of the ultrahydrophobic properties of the surface occur as the spacing between the microposts is increased beyond about 64 µm" (Ou et al., 2004). The film made using RB5 aerogels is not hydrophobic (approximately 130°), which might be due to the fact that the spacing between the aerogel material is greater than 64 µm. A review of the literature also makes me think that the tips of the aerogel material that are coming into contact with the water

on the RB2 film are similar to the etched surfaces having patterned microposts. This can be seen in Figure 2.5 with the feathery, crystalline appearance of the RB2 powder. The RB5 powder (Figure 2.6) had no definitive shape, and thus did not resemble a micropost with defined height. When taking the SEM images, the stage was tilted in an effort to quantify the height of the aerogel material on the slides. The height could not be measured, however, since the tilt angle of the stage was limited.

The SEM images revealed interesting characteristics about the powders and films on the microscale. They also illustrated how the aerogel was meshing with the Nafion in the films. Figure 2.12 shows how the films are meshing with the Nafion on a macro-level.

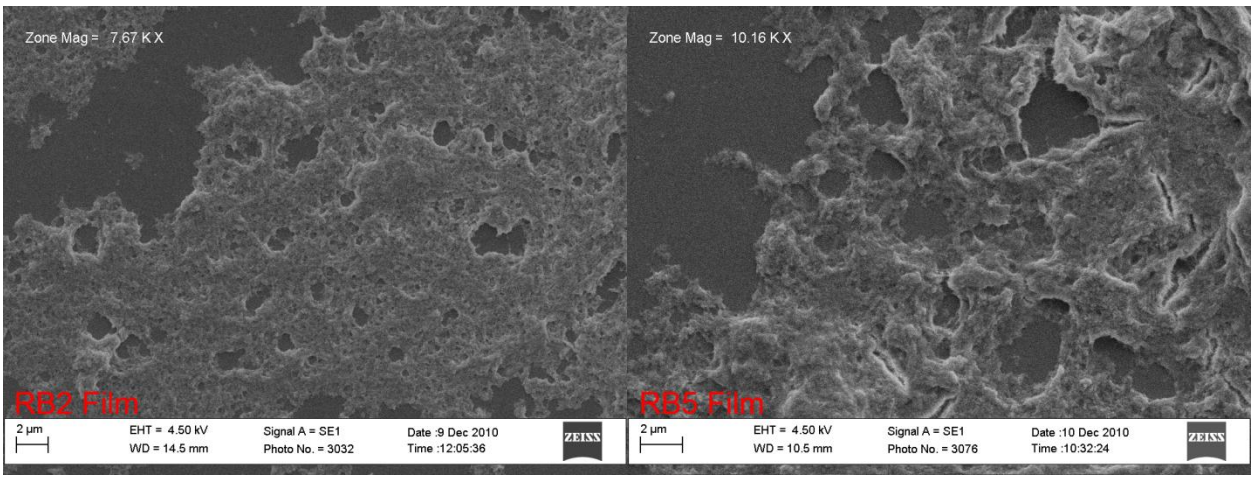

Figure 2.12: SEM images of RB2 (left) and RB5 (right) (courtesy of Nick Dunn)

In an effort to understand how the Nafion was interacting with the aerogel material, a BET surface area and BJH pore distribution test was performed on material scraped from coated glass slides using and Accelerated Surface Area and Porosimetry Analyzer. The results from this test are shown in Figure 2.13.

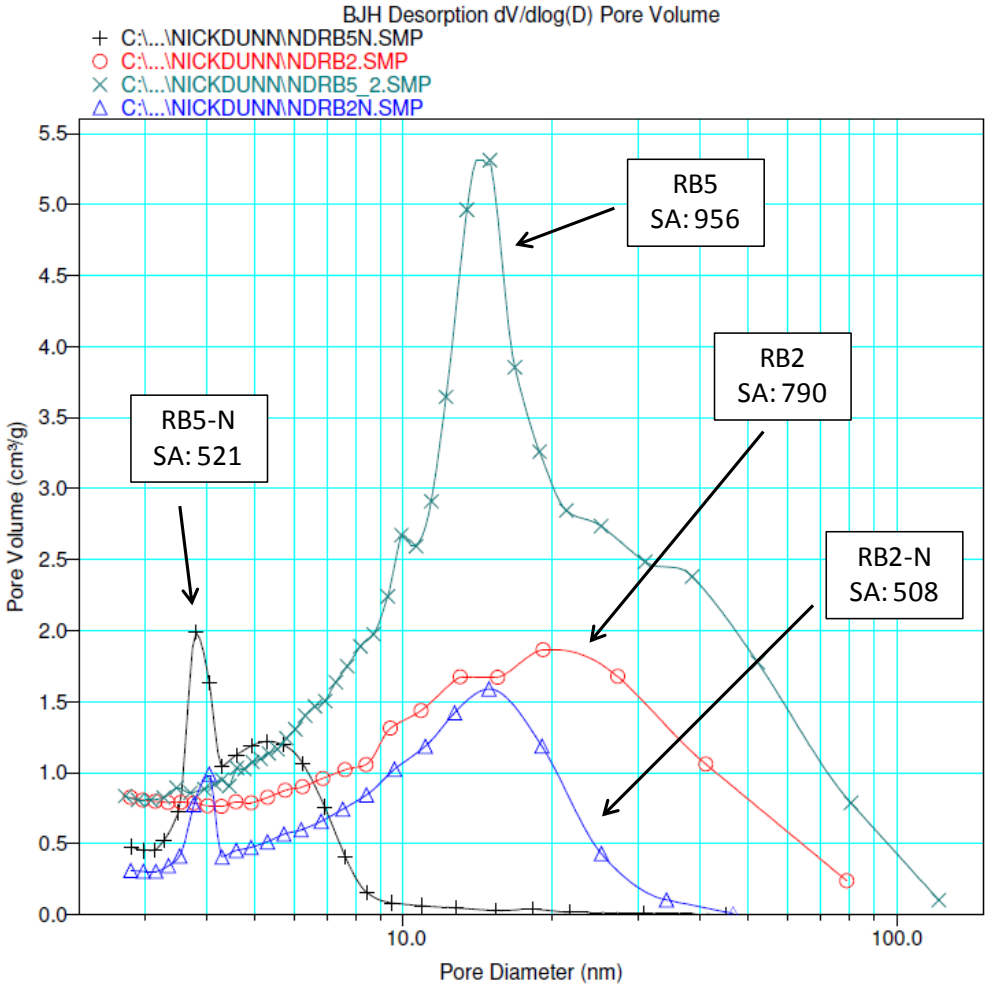

Figure 2.13: Surface area and pore distribution results for RB2 and RB5 (powders) and RB2-N and RB5-N (material from films)

The pore distribution results show that for both RB2 and RB5, the addition of Nafion eliminates a significant amount of the pores with large diameters. The effect of adding the Nafion is more pronounced with RB5. Perhaps the filling of the larger aerogel pores is what causes the surfaces to be less hydrophobic. Unfortunately these results don't show if the pores have been completely filled with Nafion, or only partially filled. The surface area decreased significantly between the powders and the film material for both RB2 and RB5. It is interesting that material from both slides had a similar surface area after Nafion was added. In addition to looking at the aerogel-Nafion interface, an investigation by

Nick Dunn (Union College, 2011) using X-Ray Diffraction showed that no significant differences exist between the "successful" and "unsuccessful" aerogel in terms of crystallinity; all samples examined were amorphous.

In summary, a superhydrophobic aerogel film was fabricated that had an average contact angle with water of 160°. This film was 250% aerogel by weight to Nafion, and was applied to a glass microscope slide using a paintbrush. The most uniform powders were fabricated by crushing with a mortar and pestle, using propanol as a solvent. The most successful Nafion solution was 5 wt. % polymer content, 15 – 20 wt. % water, and 75 wt. % alcohol (propanol). Simply using superhydrophobic aerogels is not enough to make quality superhydrophobic films. Aerogels that are not pre-gelled during the fabrication process produce films with significantly higher hydrophobicity than films using aerogels that have been pre-gelled. The most hydrophobic films had a uniform distribution of aerogel material on the slide, small gaps between aerogel material, and a feathery, crystalline structure at the peaks of the aerogel material coming in contact with water. Future work with these surfaces should include experimenting with difference materials to bind the aerogel powder to surfaces. Nafion might not be the best material to use for this type of application.

Chapter 3: Falling Ball Experiment

This chapter reviews the first of a series of three experiments that were performed to quantify the drag on coated surfaces. A falling ball experiment was performed that quantifies the drag forces on coated balls falling through water. The objectives of the experiment, theory, methods and materials, results, and discussion are included. Additional information can be found in the appendices.

Experimental Objectives

The objectives of this experiment were to determine if a difference in falling velocity is observed between uncoated and coated balls of the same weight, and to determine if coating the balls has an effect on the coefficient of drag over a range of Reynolds numbers.

Theory

Originally this experiment was designed for balls falling vertically downward through static water. During preliminary testing, however, it was determined that the falling behavior of the balls was quite unpredictable due to vortex shedding from the ball, which caused it to "wobble" as it fell. The falling behavior was

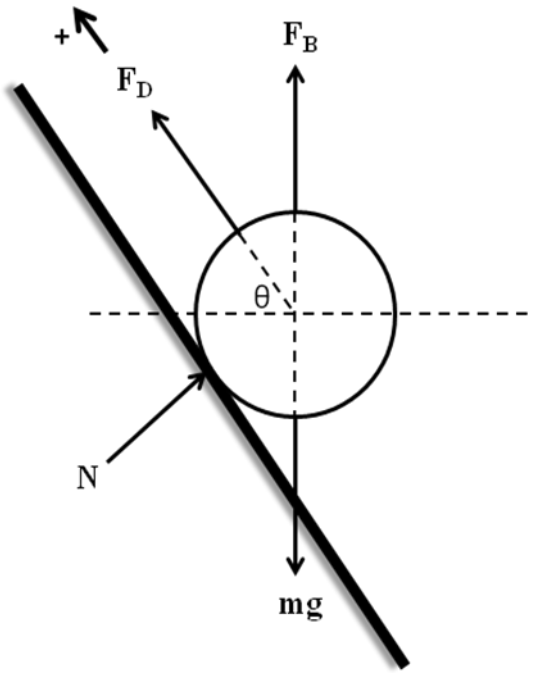

Figure 3.1: Free body diagram

normalized, however, by tilting the graduated cylinder on an angle, allowing the ball to glide down the submerged inclined surface. Figure 3.1 shows the free body diagram of the ball while it is gliding down the inclined wall of the graduated cylinder. The normal force, N, acts perpendicular to the motion of the ball and therefore has no effect on the motion of the ball. The buoyancy force, F_B, is defined by Equation 3-1,

$$F_B = \rho_w V g \tag{3-1}$$

where, ρ_w is the density of the water, V is the volume of the ball, and g is the force of gravity. It was determined during the analysis of the experiment that calculating the buoyancy of the ball based on the volume of fluid displaced, as done in Equation 3-1, was not accurate. Instead, the weight of the balls had to be measured in water. This phenomenon will be discussed in a later section. According to Newton's second law of motion (Equation 3-2),

$$F = ma \tag{3-2}$$

the force on an object is equal to the mass of the object multiplied by the acceleration of the object. For this experiment it was desirable to observe the behavior of the ball once it had reached terminal velocity (zero acceleration). The forces on the falling ball can therefore be summed equal to zero in the indicated positive direction (Equation 3-3),

$$F_D - F_B \sin\theta - mg \sin\theta = 0 \tag{3-3}$$

where F_D is the drag force, F_B is the buoyancy force, and mg is the weight of the ball. The drag force, F_D, is therefore defined by Equation 3-4,

$$F_D = (mg - F_B) * \sin\theta \tag{3-4}$$

where $(mg - F_B)$ is the weight of the ball in water. The coefficient of drag, C_D, is defined by Equation 3-5,

$$C_D = \frac{F_D}{\frac{1}{2}\rho v^2 A} \tag{3-5}$$

where F_D is the drag force, ρ is the density of the water, v is the velocity of the ball, and A is the frontal area of the ball. The drag force on the sphere is determined by the type of fluid flow over the sphere. The type of flow is characterized by the Reynolds number (Equation 3-6),

$$Re = \frac{\rho V D}{\mu} \tag{3-6}$$

where ρ is the density of the fluid, v is the velocity of the object, D is the diameter of the sphere, and μ is the viscosity of the fluid. For this experiment it was desirable to test the ball in laminar flows (low Reynolds numbers).

Experimental Methods and Materials

The first step in performing this experiment was choosing which type of ball to use. Appendix M explains the decision process used to choose the appropriate ball based on a variety of criteria. The ping pong balls used in this experiment were standard size (diameter of approximately 40 mm). The density of the balls was increased by adding weight (inserting small steel balls though a hole drilled into the outer surface of the ping pong ball). Appendix N details the procedure for changing the density of the balls and coating them with the superhydrophobic aerogel surface coating. A graduated cylinder was the main component of the testing apparatus (see Figure 3.2). It was tilted at an angle, θ, of 70°. A stopwatch was used to manually record the time for the ping pong ball to fall 7 inches (0.1778 m). A magnet was used to remove the ball from the graduated cylinder after each trial. Only trials where the ball glided smoothly down the inclined surface were recorded. This process was repeated for both coated and uncoated ping pong balls. Table 3.1 summarizes the physical properties of each ball.

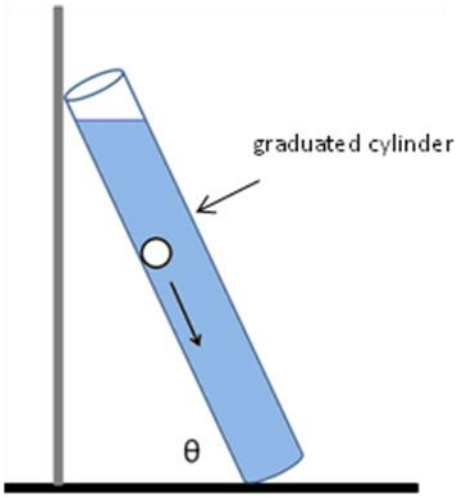

Figure 3.2: Experimental Schematic

Table 3.1: Summary of the physical properties of the ping pong balls

	Ball A		Ball B		Ball C		Ball D	
	uncoated	coated	uncoated	coated	uncoated	coated	uncoated	coated
diameter (cm)	4.064		4.057		4.046		4.066	
weight in air (g)	32.779	32.794	33.030	33.048	33.223	33.237	33.418	33.462
weight in water (g)	0.582	0.543	0.961	0.871	1.251	1.165	1.185	1.173

Results

The effect of coating the balls was observed as soon as the balls were submerged in water. The superhydrophobic aerogel coating trapped a layer of air between the surface of the ball and the water (seen in Figures 3.3 and 3.4).

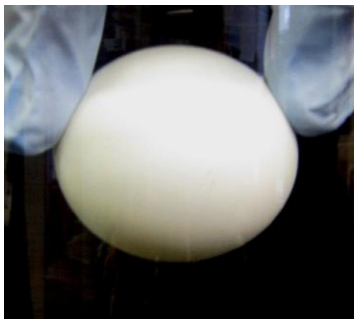

Figure 3.3: Uncoated ping pong ball submerged in water

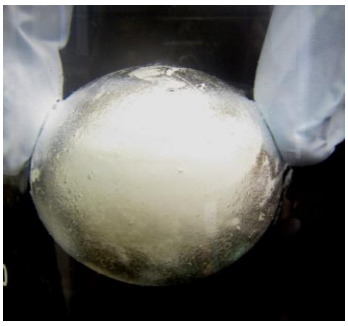

Figure 3.4: Coated ping pong ball submerged in water

Table 3.2 summarizes the results obtained for each ball. Additional data can be found in Appendix O.

Table 3.2: Results from the falling ball experiment

	Ball A		Ball B		Ball C		Ball D	
	uncoated	**coated**	**uncoated**	**coated**	**uncoated**	**coated**	**uncoated**	**coated**
average time (s)	3.57	3.73	2.68	2.98	2.37	2.54	2.31	2.56
average velocity (m/s)	0.050	0.048	0.066	0.060	0.075	0.070	0.077	0.070
average Re	2018	1930	2681	2411	3018	2816	3118	2818
F_D (N)	0.0054	0.0050	0.0089	0.0080	0.0115	0.0107	0.0115	0.0108
average C_D	3.3	3.4	3.1	3.5	3.2	3.4	3.0	3.5

During summer research, odd trends in the falling behavior of the balls were observed with increasing number of time trials. Figures 3.5 – 3.8 show the falling behavior of the balls during experiments from the first semester of this project. These figures show that the falling behavior of the balls was able to be regulated; no significant trends were observed.

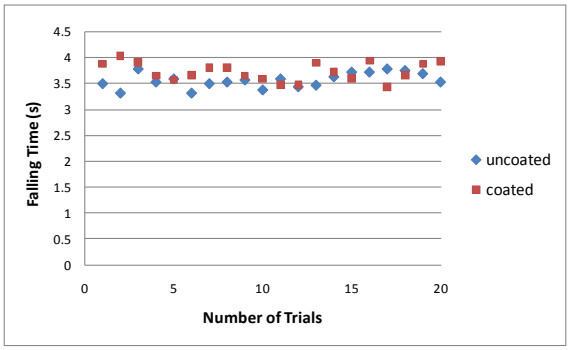

Figure 3.5: Falling behavior of Ball A

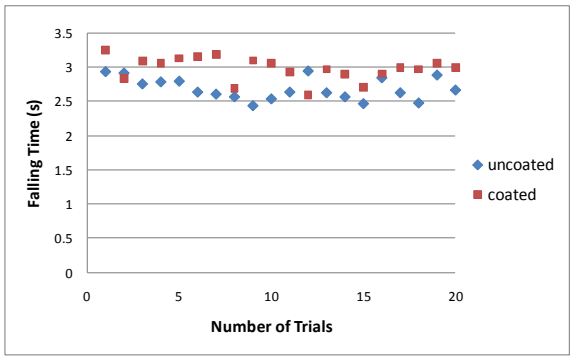

Figure 3.6: Falling behavior of Ball B

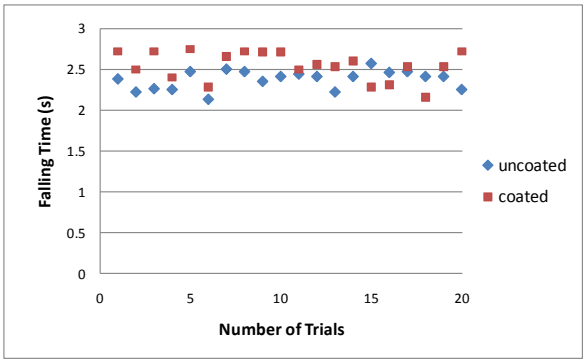

Figure 3.7: Falling behavior of Ball C

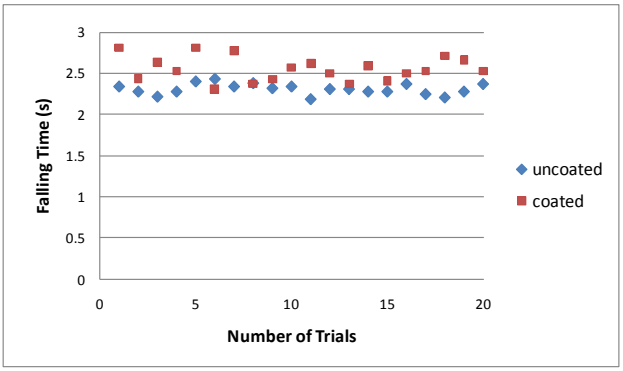

Figure 3.8: Falling behavior of Ball D

The main results from the final experiment are shown in Figure 3.9.

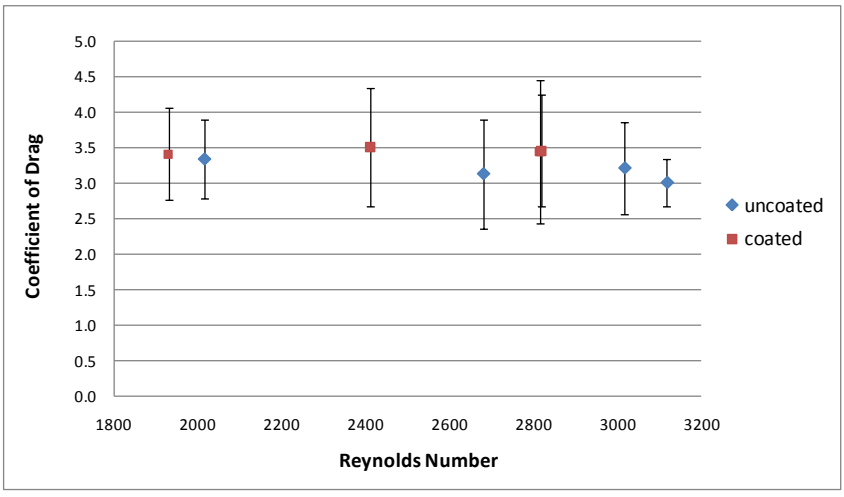

Figure 3.9: Coefficient of drag versus Reynolds number

The uncertainty in the coefficient of drag was determined using the uncertainty in the velocity of the ball, the diameter of the ball, and the mass of the ball. The uncertainty in the diameter and mass of the balls was small compared the uncertainty in the velocity. The uncertainty in the velocity was calculated using two times the standard deviation of the velocity measurements.

Discussion

A significant trend was not observed in the coefficient of drag with increasing Reynolds numbers. The uncertainty was large, up to 30% for some of the balls, due to the uncertainty in the velocity. Even if the uncertainty was lower, it would be hard to determine whether any differences in coefficient of drag are present. The time was recorded manually using a stopwatch. If this experiment were repeated, I suggest using a more accurate method for timing the balls, such as laser detection. Many unexpected challenges arose while performing this experiment. The first was the irregular falling behavior of the balls. This was normalized, however, by tilting the graduated cylinder at an angle. The main challenge was overcoming the buoyancy force. The buoyancy force was originally calculated using the volume of water that was displaced by the ball. However when this buoyancy force was used, a negative coefficient of drag was calculated for each of the balls. I believe the layer of air trapped on the surface of the ball by the superhydrophobic aerogel coating made this calculation inaccurate compared to what was physically occurring. The accurate buoyancy force was obtained by measuring

the weight of the balls while they were submerged in water using an analog balance scale. The layer of air trapped on the surface also increased the frontal area of the ball, which was not accounted for during the Reynolds number calculations. It was too difficult to measure the increase in the diameter of the balls caused by the layer of air. The main conclusion that can be drawn from this experiment is that the buoyancy force affected the ability to measure any effects on drag due to strictly to hydrophobicity. If this experiment were to be repeated, the falling distance of the balls should be lengthened. At the Reynolds numbers tested (1930 – 3118), the flow over the balls was dominated by pressure drag. Future experiments might include examining the wake of these falling balls.

Chapter 4: Rotational Viscometer Experiment

This chapter reviews the second experiment, which used a rotational viscometer to quantify the effect that coating a rotating spindle with superhydrophobic aerogel coating had on the drag forces exerted on the spindle. The objectives of the experiment, theory, methods and materials, results, and discussion are included. Additional information can be found in the appendices.

Experimental Objective

The objective of this experiment was to determine if a difference in torque was observed between uncoated spindles and spindles coated with superhydrophobic and non-hydrophobic aerogel over a range of Reynolds numbers. The torque required to rotate the spindle was directly related to the drag force acting on the spindle.

Theory

A rotational viscometer measures the torque required to rotate an object in a fluid at a known speed. The viscosity of a fluid can therefore be measured using the principle that the torque required to rotate an object in a fluid is a function of the viscosity of that fluid. This experiment analyzed the difference in the torque produced by metal spindles, coated with superhydrophobic as well as non-hydrophobic aerogel, rotating in water (of

known viscosity). In theory, coating a spindle with a superhydrophobic coating would decrease the resistance on the spindle while it is rotating, thus reducing the drag.

Experiments have shown that superhydrophobic surfaces tested in rotational flows have produced a drag reduction. One notable experiment, performed by Truesdell et al. (2006), used a strain controlled rheometer to measure the drag reduction in a couette cell apparatus. The surfaces were prepared using a superhydrophobic aerogel film coating that was applied to a patterned substrate. This particular experiment yielded a 20% drag reduction, which the authors attributed to macroscopic slip. Sean Maginess (Union College, 2008) designed and conducted a similar experiment that involved attaching an aerogel to a spindle of a Brookfield Dial LVT Viscometer. He observed a slight reduction in drag using Scotch heavy-duty mounting tape to secure the aerogel to the spindle.

Rotational viscometers operate at pre-set speed increments, therefore it was necessary to relate these speeds to the Reynolds number of the flow over the spindle. The type of flow can be characterized by the Reynolds number (Equation 4-1),

$$Re = \frac{\rho v D}{\mu} \qquad (4\text{-}1)$$

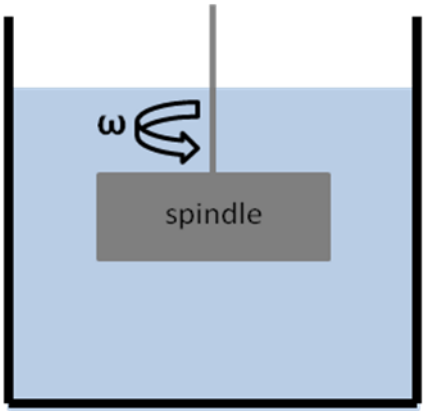

Figure 4.1: Experimental Schematic

where ρ is the density of the fluid, $\mathbf{v}$ is the velocity of the object, D is the diameter of the spindle, and μ is the dynamic viscosity of the fluid. The velocity at the edge of the spindle, $\mathbf{v}$, was calculated using Equation 4-2,

$$v = \frac{\pi \cdot D \cdot RPM}{60} \qquad (4\text{-}2)$$

where D is the diameter of the spindle, and RPM is the speed of rotation. Two stainless steel spindles were used during this experiment. Appendix P shows images of the spindles, including dimensions. Prior to testing, it was necessary to determine the Reynolds number of the flow over the spindles at each rotational speed. Table 4.1 summarizes the flow conditions that were used during testing.

Table 4.1: Flow conditions during testing; assumed density of water to be 998 kg/m^3 and dynamic viscosity to be 1×10^{-3} Pa-s

Spindle S01			Spindle S02		
RPM	**velocity (m/s)**	**Re**	**RPM**	**velocity (m/s)**	**Re**
5	0.015	855	5	0.012	592
10	0.030	1710	10	0.025	1184
20	0.060	3419	20	0.050	2368
30	0.090	5129	30	0.075	3552
50	0.150	8549	50	0.125	5920
60	0.180	10258	60	0.150	7104
**out of range*			100	0.249	11840

Experimental Methods and Materials

A LVDVE Brookfield Viscometer (Serial Number: E6515568) was used for this experiment (shown in Figure 4.2)

.

Figure 4.2: LVDVE Brookfield Viscometer

A large beaker was filled with water, and the spindle was submerged into the beaker. A digital read-out on the viscometer displayed the percent torque required to rotate the spindle at the given rotational speed. A stopwatch was used to manually record the torque every ten seconds for ten readings. It was important to allow the viscometer to stabilize at each rotational speed for approximately one minute before recording the torque. A detailed procedure is included in Appendix Q.

Two spindles with large surface areas were selected to use for this experiment, Spindle S01 and Spindle S02 (see Appendix P for spindle specifications). A preliminary experiment was conducted to determine if the viscometer could test the surface coatings at high Reynolds numbers using these spindles. The results from this experiment are shown in Figure 4.3.

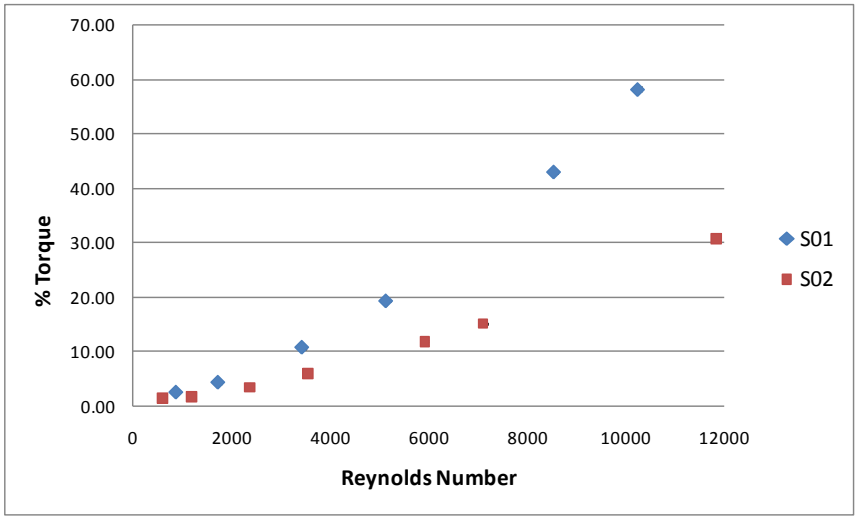

Figure 4.3: Percent torque versus Reynolds number;
preliminary testing of uncoated spindles S01 and S02

It is worth noting that the accuracy of the viscometer is significantly decreased when the percent torque is below 10%, therefore the spindles could only be accurately tested at 30, 50, and 60 rpm. After additional testing, it was determined that Spindle S02 did not have enough surface area for the coatings to affect the torque on the spindle, so for the remainder of the experiment only Spindle S01 was used.

It is worth mentioning that the viscosity of water could not be accurately measured using these spindles due to the low viscosity of water (Cp of approximately 1.0). Rotational viscometers are generally used to determine the viscosity of viscous fluids. At 60 rpm, Spindle S01 measured an average Cp of 9.1.

After preliminary testing, it was determined that the torque required to rotate the spindle was affected by the size of the beaker and the temperature of the water. The flow of water over the rotating spindle was disturbed if the spindle was positioned too close to the wall of the beaker. Two beakers were used during the experiment, 600 ml and 1000 ml volume. The 1000 ml beaker, used for the final experiments, had a larger diameter than the 600 ml beaker, which increased the distance between the rotating spindle and the

wall of the beaker. The temperature of the water also had a significant effect on the behavior of the spindle. Rotational viscometers are normally used to measure the viscosity of a fluid, a property that is highly dependent on temperature. Percent torque data collected at different temperatures cannot be directly compared, since the properties of the water are different at different temperatures. To eliminate differences in the temperature of the water, a final experiment was performed at constant water temperature.

The spindle was tested without a coating, with superhydrophobic aerogel coating, and with non-hydrophobic aerogel coating (TMOS aerogel) to determine if the surface texture in addition to hydrophobicity had an effect on the behavior of the spindle. A coated spindle has a different surface texture than a smooth, uncoated spindle. A variety of experiments were performed at varying water temperatures (changes in room temperature) using different batches of aerogels. The hydrophobicity of the coatings was quantified by contact angle measurements taken with a Kruss Drop Shape Analyzer (DSA 100).

Results

During preliminary experiments it was determined that only Spindle S01 could be used for this experiment due to its large surface area. The spindle was tested uncoated and coated with aerogel film from RB5, RB7, and TMOS aerogels (courtesy of Shira Mandel, Union College, 2005). The experiments have been summarized in Table 4.2.

Table 4.2: Summary of experiments performed with rotational viscometer

Experiment	Water Temp	Beaker	Procedure	Coating	Material	Application	Avg. CA	CA St. Dev.
#1: UNC - 1	19.0 °C	600 ml	preliminary	no	-	-	-	-
#2: RB7 - 1	19.0 °C	600 ml	preliminary	yes	RB7	paintbrush	SSH	-
#3: UNC - 2	18.5 °C	600 ml	preliminary	no	-	-	83°	4°
#4: RB7 - 2	18.5 °C	600 ml	preliminary	yes	RB7	makeup sponge	147°	11°
#5: RB7 - 3	19.0 °C	600 ml	preliminary	yes	RB7	paintbrush	156°	11°
#6: UNC - 3	20.5 °C	1000 ml	final	no	-	-	-	-
#7: TMOS	21.5 °C	1000 ml	final	yes	TMOS	paintbrush	71°	16°
#8: RB7 - 4	19.0 °C	1000 ml	final	yes	RB7	paintbrush	161°	6°
#9: RB5	18.5 °C	1000 ml	final	yes	RB5	paintbrush	149°	6°
#10: RB7 - 5	18.0 °C	1000 ml	final	yes	RB7	paintbrush	151°	5°
#11: UNC - 4	18.0 °C	1000 ml	final	no	-	-	64°	10°

When submerged, coated spindles had a layer of air trapped on the surface, similar to the coated ping pong balls in the falling ball experiment. This can be seen in Figures 4.4 and 4.5 below.

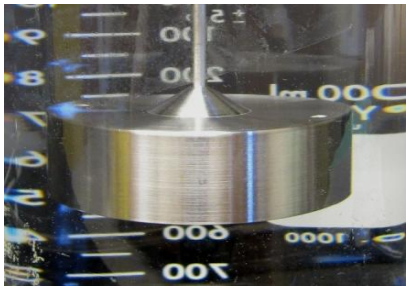

Figure 4.4: uncoated spindle submerged in water

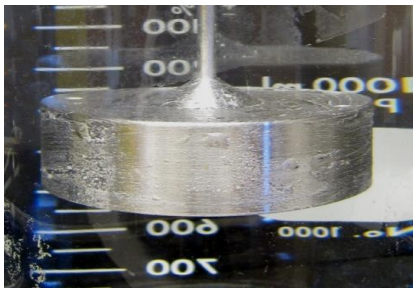

Figure 4.5: coated spindle submerged in water

The results from experiments UNC-1 and RB7-1 showed an 11% reduction in torque with the coated versus the uncoated spindle at a rotational speed of 60 rpm. Unfortunately these results were never repeated. Figure 4.6 shows percent torque versus rotational speed for preliminary experiments.

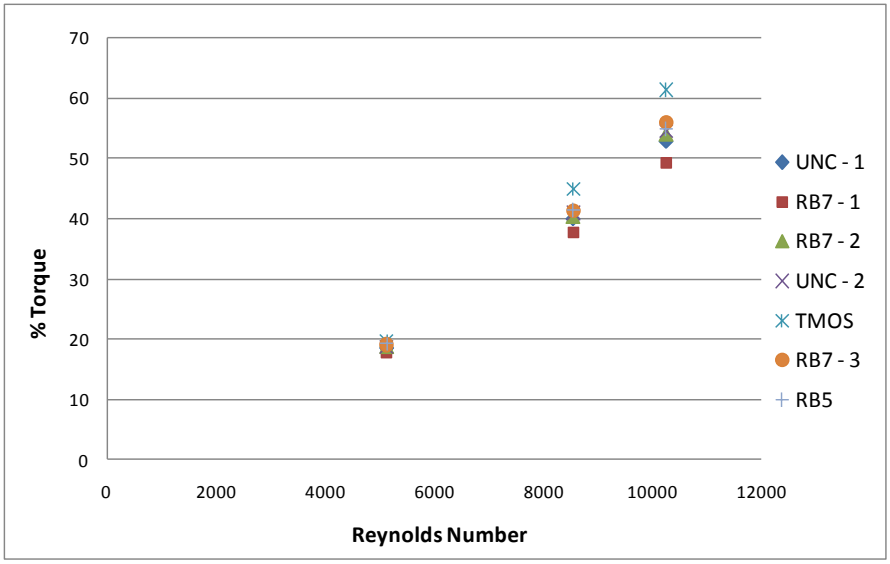

Figure 4.6: Percent torque versus Reynolds number; preliminary experiments

The most significant differences in torque were observed at a rotational speed of 60 rpm. As expected, coating the spindle with TMOS aerogel (non-hydrophobic aerogel) film increased the torque. Surprisingly, applying the aerogel film with the make-up sponge produced the greatest torque reduction. Although the make-up sponge reduced the torque, the coating was non-uniform and deteriorated quickly. The most successful application technique, as proven in the falling ball experiment, was using a paintbrush. These experiments were performed with water of varying temperatures, so it could not be concluded whether these results were solely based on the coating, or if water temperature was having an effect. It was noted that during certain experiments the torque increased with increasing number of time trials. This was believed to be due to a decrease in the hydrophobicity of the aerogel coating the longer it was submerged in the beaker of water. For each experiment the percent torque was plotted over the number of time trials to determine if visible trends formed as the data was collected. These plots are included in Appendix R, but the plot of Experiment 10: RB7-5 is shown below.

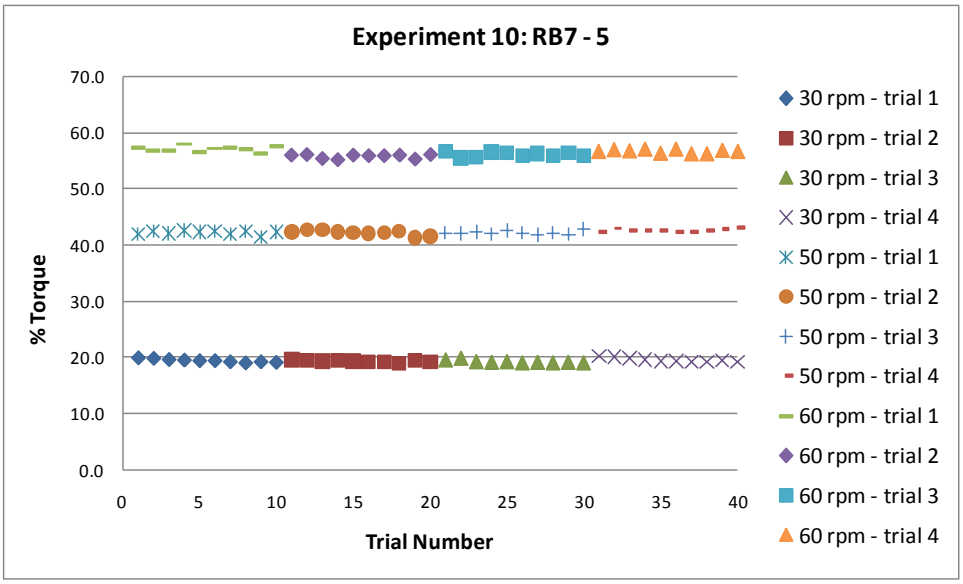

Figure 4.7: Percent torque versus consecutive time trials

For this particular experiment, the coating did not appear to deteriorate over time. When the spindle was removed from the beaker between trials 3 and 4, drops were still beading on the surface. A contact angle measurement was taken of one of the drops and found to be 151.4° (image shown below), which is consistent with the contact angle measurements taken before the experiment.

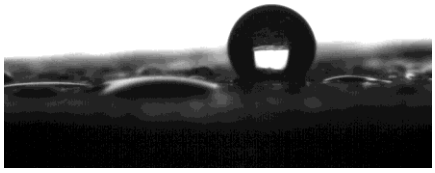

Figure 4.8: Image of a water drop on RB7 coated spindle, taken with the Kruss Drop Shape Analyzer

This image illustrates the non-uniform hydrophobicity of the surface coating once it had experienced prolonged water exposure. Notice that drops have wetted the surface only a short distance from the hydrophobic area.

A final experiment was conducted to determine if temperature was in fact affecting the results. A plot of percent torque versus Reynolds number is shown in Figure 4.9.

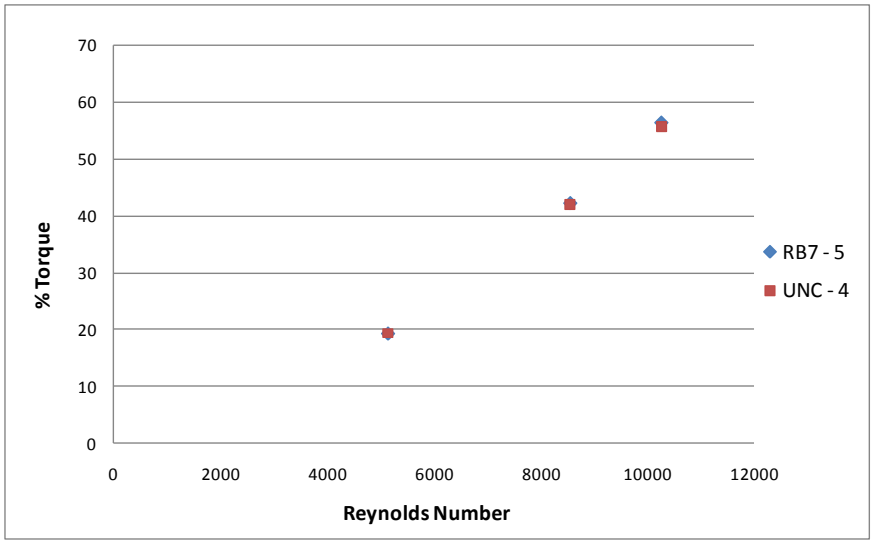

Figure 4.9: Percent torque versus Reynolds number; water temperature of 18 °C

The uncertainty in the percent torque measurements was low; the standard deviation in percent torque ranged from 0.2 to 0.56 % for the final experiment. This experiment confirmed that there was no significant difference in torque for a coated versus uncoated spindle tested in water of the same temperature.

Discussion

This experiment increased the range of Reynolds numbers tested from the previous falling ball experiment. For rotational flows at the Reynolds numbers tested, the drag was mostly due to friction drag. Prior to this experiment it was believed that the coatings would have a significant effect on friction drag. The results show otherwise, however.

The main conclusion that can be drawn from this series of experiments is that for the conditions tested, no significant difference was observed in the torque required to rotate a coated versus uncoated spindle. Therefore, the superhydrophobic aerogel coating did not affect the drag forces on the spindle. There are a few explanations for the results obtained in these experiments. The effects of the surface coatings were most significant at higher Reynolds numbers, and barely noticeable at low Reynolds numbers. It may be possible that the limitations of the experimental apparatus (size of the spindle and rotational speed of the viscometer) are preventing significant differences in the torque from being observed. The size of the beaker could also be affecting the flow. Ideally, a large container should be used to hold the water so the spindle would be far from the walls of the container and the water would only be affected by the rotation of the spindle.

The surface coating may also be affecting the results. During each experiment a considerable amount of aerogel material was removed from the surface of spindle while it was rotating in the water. It is possible that the coating deteriorates and the hydrophobicity is decreased with increased water exposure. Alternative chemicals should be considered to bind the aerogel surfaces. Nafion may not be the best chemical to use for coatings that are submerged in water.

If this experiment were to be repeated, the most critical variable to regulate would be water temperature. It appears that even slight fluctuations in temperature can have a significant effect on the torque required to rotate the spindle. Another variable to consider is the size and shape of the spindle. A custom spindle could be machined to maximize surface area.

Chapter 5: Particle Image Velocimetry Experiment

This chapter reviews the third and final experiment that used Particle Image Velocimetry (PIV) to analyze the wake region of cylindrical test pieces in cross flow that had been coated with superhydrophobic aerogel coating. The objectives of the experiment, theory, methods and materials, results, and discussion are included. Additional information can be found in the appendices.

Experimental Objective

The objective of this experiment was to determine if a cylinder in cross flow, coated with superhydrophobic aerogel coating, produces a smaller wake size than an identical, uncoated cylinder tested at the same flow conditions. Different sized cylinders were used to examine the effects of the coating over a range of Reynolds numbers. This experiment involved redesigning and constructing a circulating water tank which was used as the test apparatus for this experiment.

Theory

A circulating water tank was used to examine the wake region of circular cylinders in cross flow. The cylindrical test pieces were aligned so that the free stream flow in the tank was perpendicular to the axis of the cylinder. The flow pattern around

cylinders in cross flow can vary significantly depending on the Reynolds number. The Reynolds number is shown in Equation 5-1,

$$Re = \frac{\rho v D}{\mu} \tag{5-1}$$

where ρ is the density of the fluid, $\mathbf{v}$ is the velocity of the fluid, D is the diameter of the cylinder, and μ is the dynamic viscosity of the fluid. Cylindrical test pieces of four diameters were fabricated. The flow conditions over each test piece is summarized in Table 5.1. The Reynolds number range of this experiment is lower than that tested by the falling ball and rotational viscometer experiments.

Table 5.1: Summary of flow conditions for test pieces

cylinder	diameter	Re
1	3/8 in	613
2	1/2 in	818
3	3/4 in	1226
4	1 in	1635

These Reynolds numbers were calculated using a free stream velocity in the tank, $\mathbf{v}$, of 0.0645 m/s, and a flow rate, Q, of 1.9×10^{-4} m/s. The velocity in the tank was computed by physically measuring the flow rate through the tank, then using Equation 5-2, where Q is flow rate, A is the cross-sectional area of the flow, and $\mathbf{v}$ is the velocity of the flow.

$$\mathrm{Q} = \mathrm{A} \times \mathbf{v} \tag{5-2}$$

The density of the water, ρ, was assumed to be 998 kg/m^3 and the dynamic viscosity, μ, was assumed to be 1×10^{-3} Pa-s. At these Reynolds numbers, the flow over the test pieces is laminar. When the test pieces are placed in cross flow, a wake region is produced behind the cylinder. This is due to a low pressure region where the fluid particles have slowed and lost momentum. Figure 5.1 illustrates how this wake region is formed.

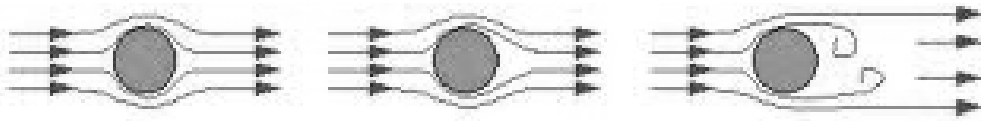

Figure 5.1: Wake formation behind a circular cylinder in cross flow
(courtesy of <http://mechse.illinois.edu>)

In theory, the size of the wake would be decreased if a superhydrophobic surface coating was applied to the cylinder. Superhydrophobic surfaces create a layer of air between the surface and the fluid. This should increase the velocity of the particles moving over the cylinder, induce earlier separation of the boundary layer, and reduce the size of the wake.

Particle Image Velocimetry (PIV) was used to analyze the wake region. PIV uses a double pulsed laser to track the path of particles in a fluid flow. A schematic of a PIV test apparatus is shown in Figure 5.2.

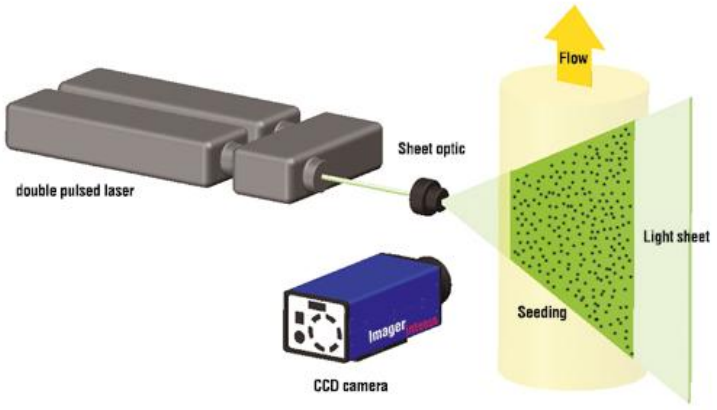

Figure 5.2: Experimental schematic of PIV
(courtesy of <http://www.piv.de/images/content/piv_components.jpg>)

The displacement of these particles is calculated using two-dimensional vector fields. These vector fields indicate the velocity of particles in the entire section of flow being examined, including the wake region. Generally the flow is seeded with particles that can easily be detected when they are illuminated by the laser. For this experiment, the flow was not seeded. Dust particles in the water were large enough to be detected by the camera.

Experimental Methods and Materials

Prior to the start of experimental testing, the circulating water tank was redesigned and constructed. The old flow tank, used by Sean Maginess (Union College, 2008) was broken and unusable. The new tank, shown in Figure 5.3, was designed with several objectives in mind: the entire apparatus must be water-tight, the design must be compatible with PIV testing, and the test pieces must be mounted so they can be easily interchanged during testing.

Figure 5.3: Circulating water tank

The flow chamber is 24” long, with a cross section of 2.5” by 2.5”, made of 3/8” polycarbonate. PVC stock and rubber gasket material were secured onto the ends of the flow chamber with threaded steel rods. The inlet of the flow chamber contains a flow

straightener; a section of plastic straws, glued together and held in place with metal screens. The water tank is connected to a magnetic drive pump using 1/2” tygon tubing. The pump was purchased from Aquatic Eco-Systems, Inc. (Model#: MD7) and is rated for 700 GPH. A plastic container was used to hold the pump and additional water during testing. The test pieces are 2.5” long polycarbonate cylinders (shown in Figure 5.4).

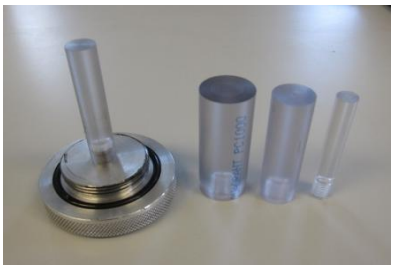

Figure 5.4: Test pieces

These cylinders are secured in the flow chamber by an aluminum mounting piece, shown in Figure 5.5.

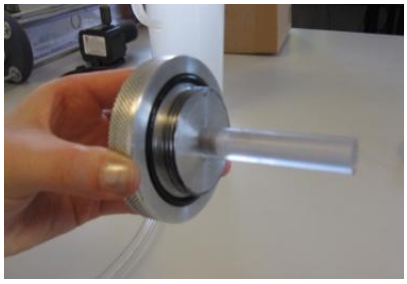

Figure 5.5: Test piece mount

This piece screws into a threaded hole in the back of the tank, and is sealed by a Buna-N O-ring (width: 1/8”, I.D:1-7/8”, O.D: 2-1/8”). The cylindrical test pieces are then screwed onto the mounting piece. The mounting piece was spray painted with flat black paint to prevent reflection from the laser during testing. Similarly, the bottom face and back face

of the tank were covered in black construction paper to minimize glare. The experimental setup is shown in Figure 5.6.

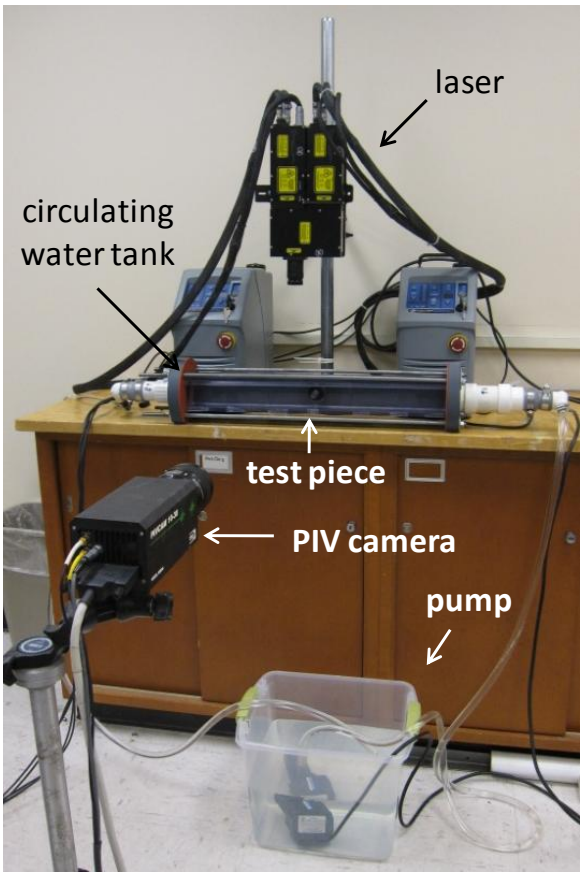

Figure 5.6: PIV experimental set-up

A TSI PIVCAM 10-30 (Model: 630046) and a 30MJ laser system from Big Sky Laser Technologies, Inc. were used to perform the experiment. They were controlled using Insight, a PIV software, from a connected computer. These systems were provided by the Union College Mechanical Engineering Department.

Two sets of test pieces were fabricated. This made it easy to interchange coated and non-coated test pieces of the same diameter during testing. The test pieces were coated with superhydrophobic aerogel film made from batch RB7 aerogels. The coating

was prepared and applied in the same manner as the previous experiments, however a detailed procedure for test piece preparation has been included in Appendix 5A. The hydrophobicity of the test pieces was examined before each experiment using the Kruss Drop Shape Analyzer. Coated cylinders consistently exhibited contact angles averaging 148°. Figure 5.7 shows one of the coated cylinders during contact angle testing.

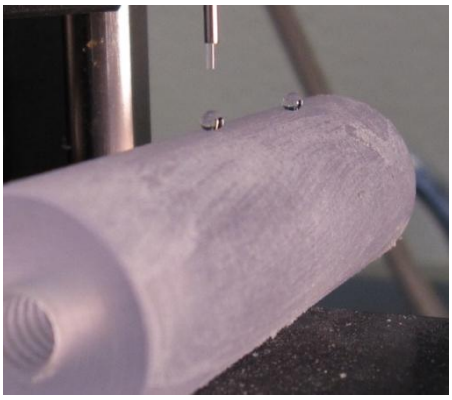

Figure 5.7: Water drops on a coated test piece

Uncoated cylinders exhibited contact angles averaging 102°. As observed in the previous two experiments, a layer of air surrounded the coated test pieces during testing. This phenomenon is shown in Figure 5.8.

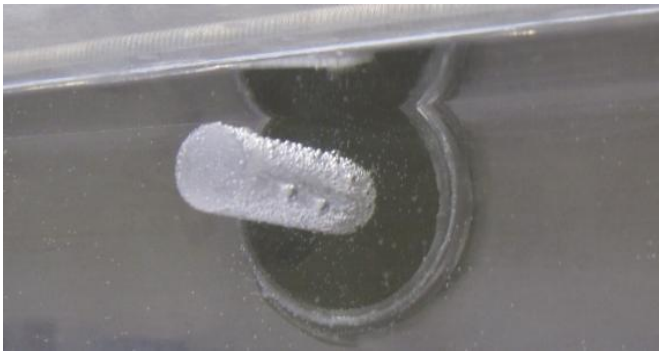

Figure 5.8: Submerged coated test piece in cross flow

The longer the test piece was submerged in water, the more bubbles formed on the surface. No bubbles formed on the surface of uncoated test pieces.

The objective of this experiment was to test two cylinders, coated and uncoated, under identical flow conditions to determine if a difference in wake size was observed. It was necessary, therefore, to setup and conduct the experiment under carefully controlled conditions. A detailed procedure for setup and testing has been included in Appendix 5B. During testing it was important that the position of the water tank remain unchanged relative to the position of the camera, as well as the laser. The laser sheet was positioned in the center of the test piece, with the center slightly downstream of the cylinder. During preliminary testing it was determined that the water only filled to a height of 2 in (out of a possible height of 2.5 in). This prevented the use of the two larger diameter test pieces.

The 1/2 in-diameter and 3/8 in-diameter test pieces were tested uncoated, coated with a single coat, and coated with a double coat. Data was collected in 350 image pairs, and was processed by applying a three standard deviation filter, twice.

Results

Figure 5.9 shows the results from the 3/8 in-diameter cylinder. Each plot represents the average vector field from 350 images.

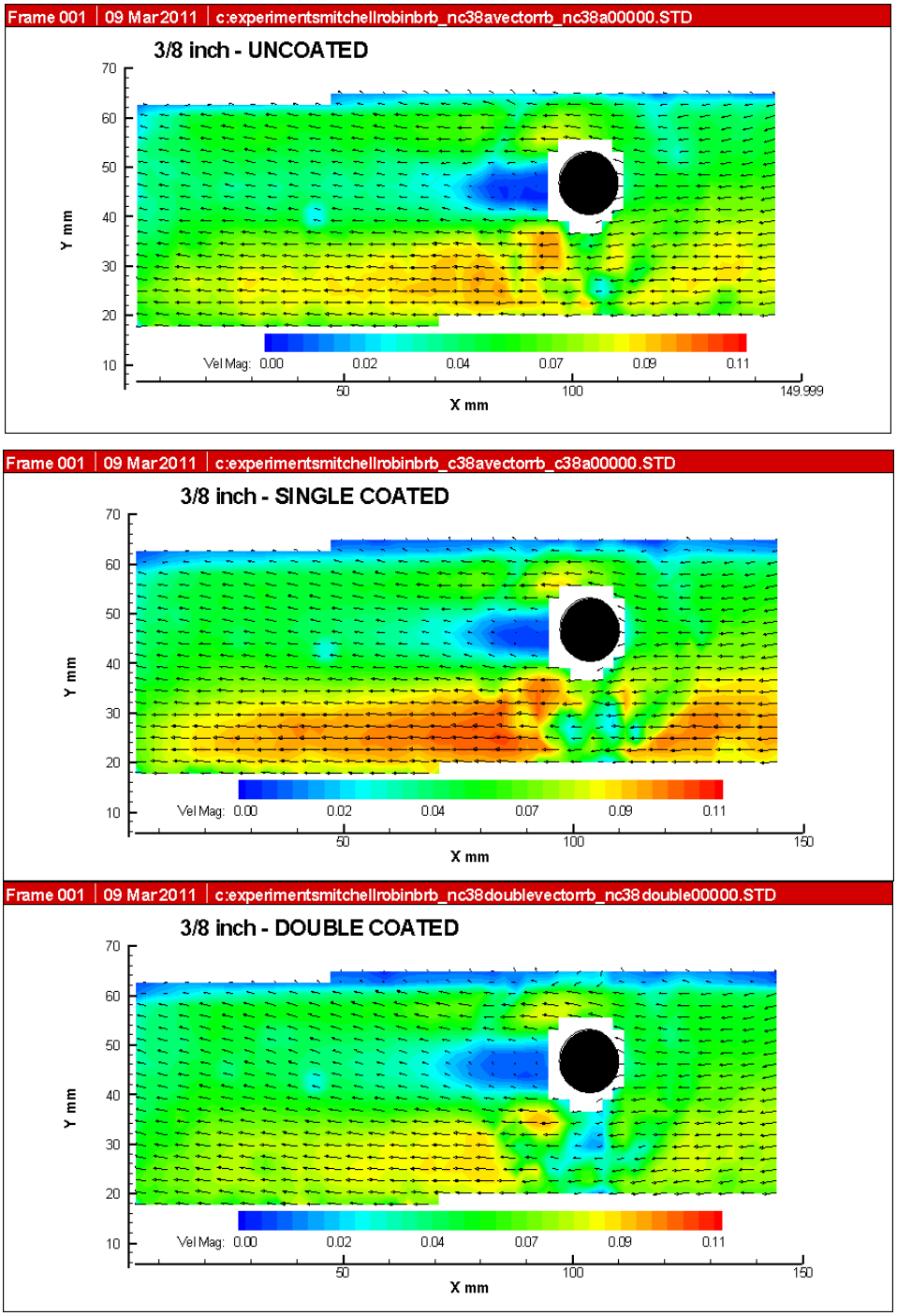

Figure 5.9: PIV results for 3/8 in-diameter test piece

Figure 5.10 shows the results from the 1/2 in-diameter cylinder. Each plot represents the average vector field from 350 images.

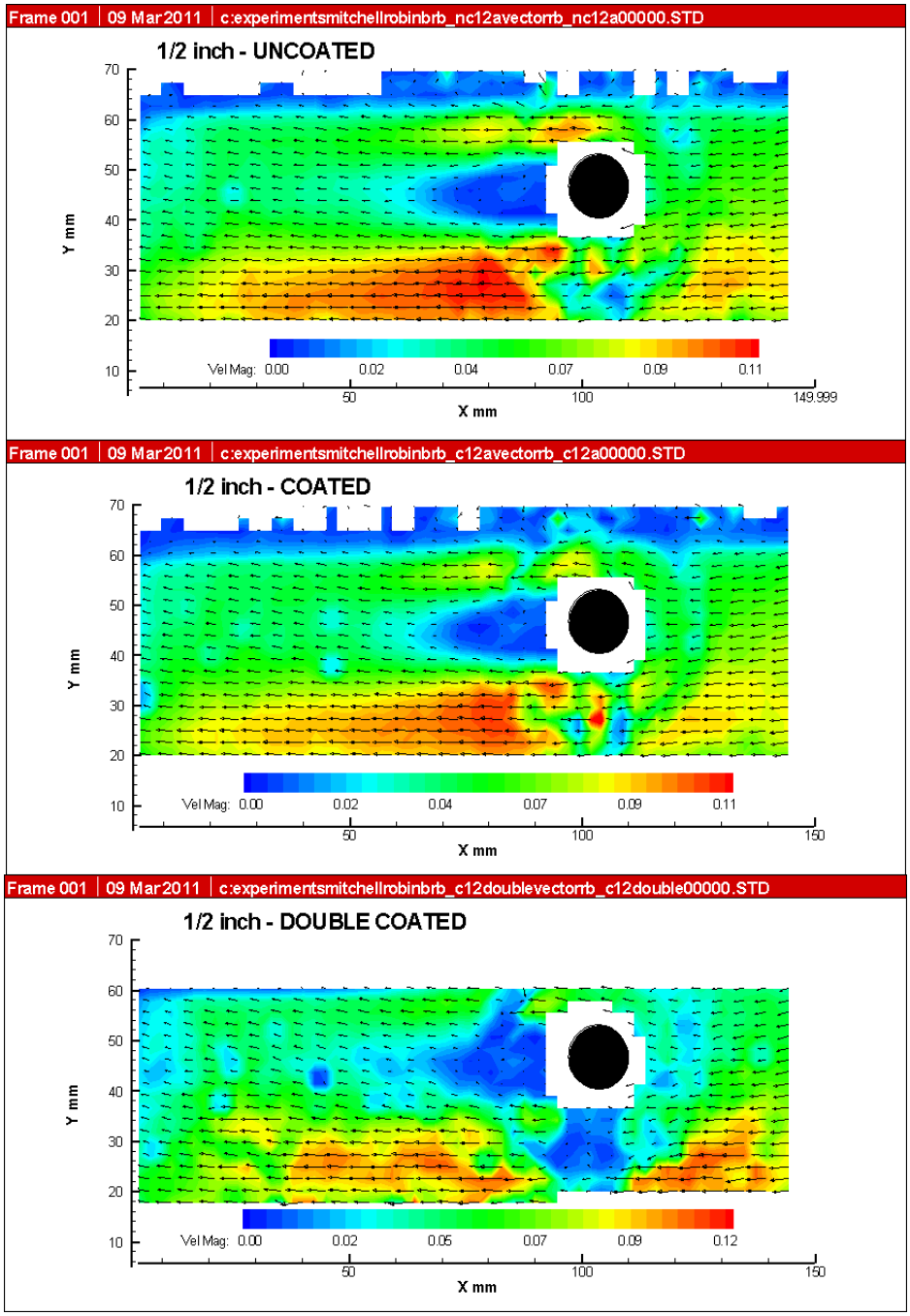

Figure 5.10: PIV results for 1/2 in-diameter test piece;
note that the intensity of the laser was reduced for the double coat experiment

It is worth noting that during the double coat test on the 1/2 in-diameter test piece, the intensity of the laser was reduced, resulting in the disturbance in the vector field plot for the double coat seen in Figure 5.10.

Discussion

The main conclusion that can be drawn from this experiment is that coating the test pieces (single or double coat) does not have an effect on the size of the wake. Once the experimental apparatus and testing procedure were finalized to ensure identical testing and imaging conditions, it was easy to visually compare the average vector field plots for each test piece. Although a slight reduction in wake size occurred when coating the 3/8 in-diameter test piece (Figure 5.9), no significant differences were observed. This experiment focused on a lower range of Reynolds numbers than the two previous experiments, and examined a combination of pressure drag and friction drag. Future PIV experiments should examine the test pieces at higher Reynolds numbers. This will include using a larger pump if the current experimental apparatus is used.

Chapter 6: Summary and Continuing Work

Over the course of this project I was able to successfully fabricate superhydrophobic aerogels, and use these aerogels to fabricate superhydrophobic aerogel surface coatings. I developed a repeatable procedure for creating these films and applying them to surfaces. During the film fabrication process I learned that the aerogel fabrication process has an effect on the hydrophobicity of films. A series of three experiments were designed and conducted to examine the effects of these surface coatings on hydrodynamic drag. The falling ball experiment and the PIV experiment tested pressure drag, while the rotational viscometer experiment tested friction drag.

Ideally, the three experiments conducted over the course of this project would have indicated superhydrophobic aerogel-based surface coatings have an effect on drag. No significant differences between coated and uncoated surfaces were observed, however. Figure 6.1 is a compilation of the results obtained in the falling ball and rotational viscometer experiments, as well as notable results from published experiments involving drag reduction over superhydrophobic surfaces, expressed as percent drag versus Reynolds number.

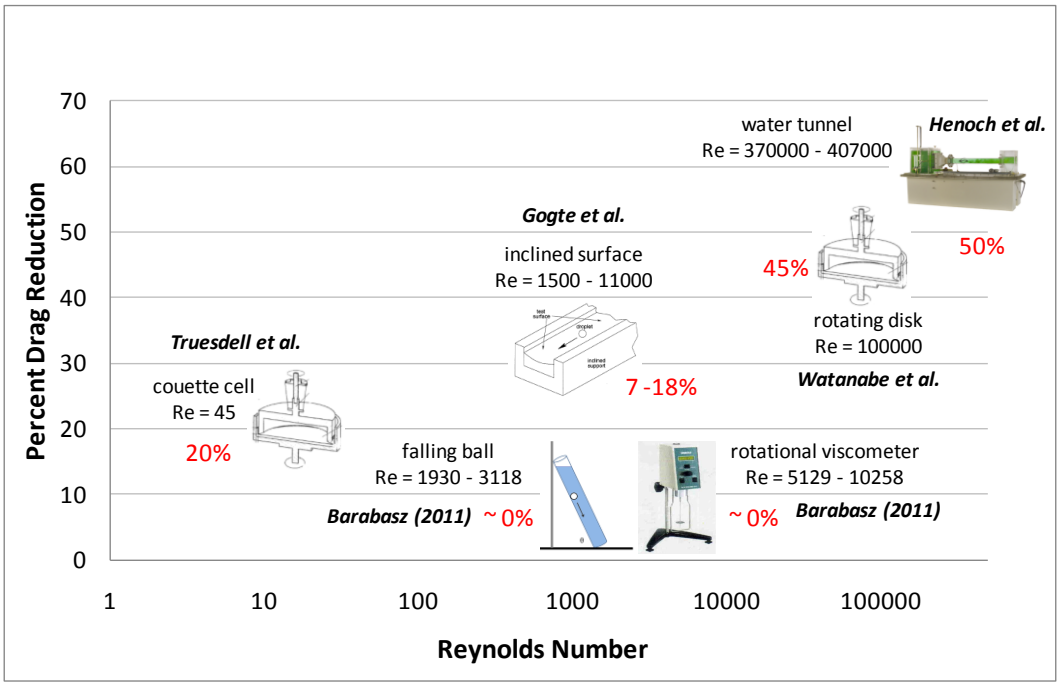

Figure 6.1: Percent drag reduction versus Reynolds number

Experiments involving superhydrophobic surfaces fabricated using photolithography techniques (those referenced in Figure 6.1) have shown that drag reduction is possible in the range of Reynolds numbers tested during this project. This gives cause to believe that the aerogel surface coatings fabricated during this project have potential to reduce drag, but that the types of experiments performed could not detect the effects.

Future work on this project should focus on two aspects: improving the aerogel surface coatings, and designing and conducting additional experiments to examine hydrodynamic drag. Nafion may not be the best material to use to bind the aerogel powder to surfaces. Other materials should be investigated that may be more suitable to this type of application. Future experiments should test the surface coatings in flows of higher Reynolds numbers, as well as design experiments that examine pressure drag and

friction drag separately. I am confident that additional experiments that test improved surface coatings will reveal a reduction in drag.

Acknowledgements

I would like to thank the following people for their contributions to this project: Union College Professors Ann Anderson, Brad Bruno, Mary Carroll, Becky Cortez, and Mike Hagerman, Rhonda Becker, Stan Gorski, Mark Hooker, Sarah Schinasi, Sean Maginess, Nick Dunn, and the Union College Machine Shop. This project would not have been possible without IEF funding, as well as NSF funding for Union's Aerogel Fabrication, Characterization, and Applications Lab (National Science Foundation Grants: NSF MRI CTS-0216153, NSF RUI CHE-0514527, NSF MRI CMMI-0722842, and NSF RUI CHE-0847901).

References

[1] Anderson, Ann M.; Carroll, Mary K.; Green, Emily C.; Melville, Jason T.; Bono, Michael S. "Hydrophobic Silica Aerogels Prepared via Rapid Supercritical Extraction." 2009. Web.

[2] Choi, Chang-Hwan; Kim, Chang-Jin. "Large Slip of Aqueous Liquid Flow over a Nanoengineered Superhydrophobic Surface." *Physical Review Letters* 96.6 (2006): 66001 (4). Web.

[3] Fukagata, Koji; Kasagi, Nobuhide; Koumoutsakos, Petros. "A Theoretical Prediction of Friction Drag Reduction in Turbulent Flow by Superhydrophobic Surfaces." *Physics of Fluids* 18.5 (2006): 051703 (4). Web.

[4] Gauthier, Ben M.; Bakrania, Smitesh D.; Anderson, Ann M.; Carroll, Mary K. "A Fast Supercritical Extraction Technique for Aerogel Fabrication." *Journal of Non-Crystalline Solids*, 350 (2004): 238 – 243.

[5] Gogte, Salil; Vorobieff, Peter; Truesdell, Richard; Mammoli, Andrea; van Swol, Frank; Shah, Pratik; Brinker, C. Jeffrey. "Effective Slip on Textured Superhydrophobic Surfaces." *Physics of Fluids* 17.5 (2005): 51701(4). Web.

[6] Henoch, C; Krupenkin, T. N.; Kolodner, P.; Taylor, J. A.; Hodes, M. S.; Lyons, A. M.; Peguero, C.; Breuer, K. "Turbulent Drag Reduction Using Superhydrophobic Surfaces." Presented 3rd AIAA Flow Control Conference, 5 – 8 June 2006. Published by the *American Institute of Aeronautics and Astronautics, Inc.*, with permission.

[7] Li, Xue-Mei; Reinhoudt, David; Crego-Calama, Mercedes. "What do we need for a superhydrophobic surface? A review on the recent progress in the preparation of superhydrophobic surfaces." *Chemical Society Reviews* 36 (2007): 1350 – 1368. Web.

[8] Ma, Minglin; Hill, Randal M. "Superhydrophobic Surfaces." *Current Opinion in Colloid and Interface Science* 11 (2006): 193 – 202. Web.

[9] Maginess, Sean. "Hydrophobic Aerogels: Reducing Hydrodynamic Drag." Union College, 2008.

[10] Min, Taegee; Kim, John. "Effects of Hydrophobic Surface on Skin-friction Drag." *Physics of Fluids* 16.7 (2004): 55(4). Web.

[11] Ou, Jia; Perot, Blair; Rothstein, Jonathan P. "Laminar Drag Reduction in Microchannels Using Ultrahydrophobic Surfaces." *Physics of Fluids* 16.12 (2004): 4635(9). Web.

[12] Ou, Jia; Rothstein, Jonathan P. "Direct Velocity Measurements of the Flow Past Drag-Reducing Ultrahydrophobic Surfaces." *Physics of Fluids* 17.10 (2005): 103606(10). Web.

[13] Rao, Venkateswara A.; Kulkarni, Manish M.; Bhagat, Sharad D. "Transport of Liquids using Superhydrophobic Aerogels." *Journal of Colloid and Interface Science*, 285 (2005): 413 – 418.

[14] Schinasi, Sarah. “The Effects of Surface Finish on Drag: Coatings of Racing Shells.” Union College, 2010.

[15] Truesdell, Richard; Mammoli, Andrea; Vorobieff, Peter; van Swol, Frank; Brinker, C. Jeffrey. “Drag Reduction on a Patterned Superhydrophobic Surface.” *Physical Review Letters* 97.4 (2006): 44504(4). Web.

Appendices

Appendix A: References for Collection of Drag Reduction Experiments

[1] Gogte, Salil; Vorobieff, Peter; Truesdell, Richard; Mammoli, Andrea; van Swol, Frank; Shah, Pratik; Brinker, C. Jeffrey. "Effective Slip on Textured Superhydrophobic Surfaces." *Physics of Fluids* 17.5 (2005): 51701(4). Web.

[2] Henoch, C; Krupenkin, T. N.; Kolodner, P.; Taylor, J. A.; Hodes, M. S.; Lyons, A. M.; Peguero, C.; Breuer, K. "Turbulent Drag Reduction Using Superhydrophobic Surfaces." Presented 3rd AIAA Flow Control Conference, 5 – 8 June 2006. Published by the *American Institute of Aeronautics and Astronautics, Inc.*, with permission.

[3] Ou, Jia; Perot, Blair; Rothstein, Jonathan P. "Laminar Drag Reduction in Microchannels Using Ultrahydrophobic Surfaces." *Physics of Fluids* 16.12 (2004): 4635(9). Web.

[4] Ou, Jia; Rothstein, Jonathan P. "Direct Velocity Measurements of the Flow Past Drag-Reducing Ultrahydrophobic Surfaces." *Physics of Fluids* 17.10 (2005): 103606(10). Web.

[5] Choi, Chang-Hwan; Kim, Chang-Jin. "Large Slip of Aqueous Liquid Flow over a Nanoengineered Superhydrophobic Surface." *Physical Review Letters* 96.6 (2006): 66001 (4). Web.

[6] Truesdell, Richard; Mammoli, Andrea; Vorobieff, Peter; van Swol, Frank; Brinker, C. Jeffrey. "Drag Reduction on a Patterned Superhydrophobic Surface." *Physical Review Letters* 97.4 (2006): 44504(4). Web.

[7] Zhao, Jia-peng; Du, Xiang-dang; Shi, Xiu-hua. "Experimental research on friction-reduction with super-hydrophobic surfaces." *Journal of Marine Science and Application* 6.3 (2007): 58(3). Web.

[8] Choi, Chang-Hwan; Westin, K. Johan A.; Breuer, Kenneth S. "Apparent slip flows in hydrophilic and hydrophobic microchannels." *Physics of Fluids* 15.10 (2003): 2897(6). Web.

[9] Watanabe, Keizo; Ogata, Satoshi. "Drag Reduction for a Rotating Disk with Highly Water-Repellent Wall." *The Japan Society of Mechanical Engineers* B41.3 (1998): 556(5). Web.

Appendix B: Superhydrophobic Aerogel Fabrication

Chemical	Amount
MTMS	6.375 ml
TMOS	6.375 ml
Methanol	41.25 ml
Water	5.40 ml
Ammonia	0.200 ml

Table B.1: 60 ml recipe

Chemical	Amount
MTMS	15.93 ml
TMOS	15.93 ml
Methanol	103.125 ml
Water	13.5 ml
Ammonia	0.507 ml

Table B.2: 150 ml recipe

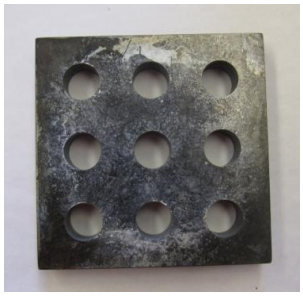

Figure B.1: Mold A

Figure B.2: Mold B

Steps	T (°F)	Rate (°/min)	Force (kips)	Rate (kips/min)	Dwell
1	90	200	48	600	3 hrs
2	550	3	48	1	30 min
3	550	200	1	1	15 min
4	90	2	1	1	30 sec

Table B.3: Hot press program 2A (pre-gel) – approximately 11 hour process

Steps	T (°F)	Rate (°/min)	Force (kips)	Rate (kips/min)	Dwell
1	90	200	48	600	3 min
2	550	3	48	1	30 min
3	550	200	1	1	15 min
4	90	2	1	1	30 sec

Table B.4: Hot press program 2B (no pre-gel) – approximately 8 hour process

Figure B.3: Temperature controlled hydraulic hot press

Figure B.4: RB2 aerogel

NOTE: RB3 aerogels looked the same as RB4 and RB5 aerogels. There were no remaining monoliths for a picture.

Figure B.5: RB4 aerogel

Figure B.6: RB5 aerogel

Figure B.7: RB6 aerogel

Figure B.8: RB7 aerogel

Appendix C: Superhydrophobic Aerogel Powders

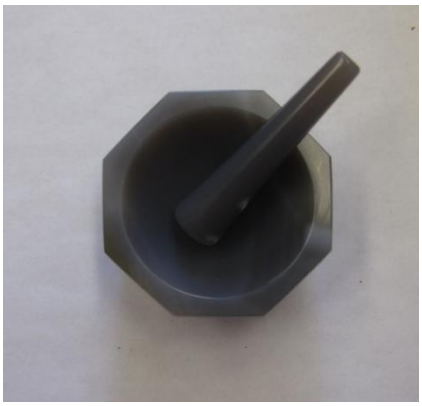

Figure C.1: Mortar and Pestle

Figure C.2: Nalgene bottle, sifter, and zirconia grinding media

Figure C.3: Ball mill

Figure C.4: Aerogel powder crushed for 20 minutes with a mortar and pestle using propanol as a solvent

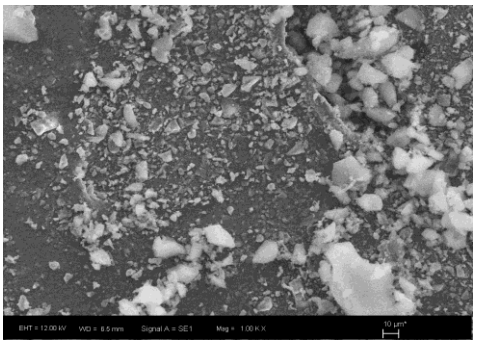

Figure C.5: SEM image (courtesy of Professor Cortez); aerogel powder crushed dry for approximately 5 minutes with a mortar and pestle

Appendix D: 10% and 50% Aerogel Dried Open in the Hood

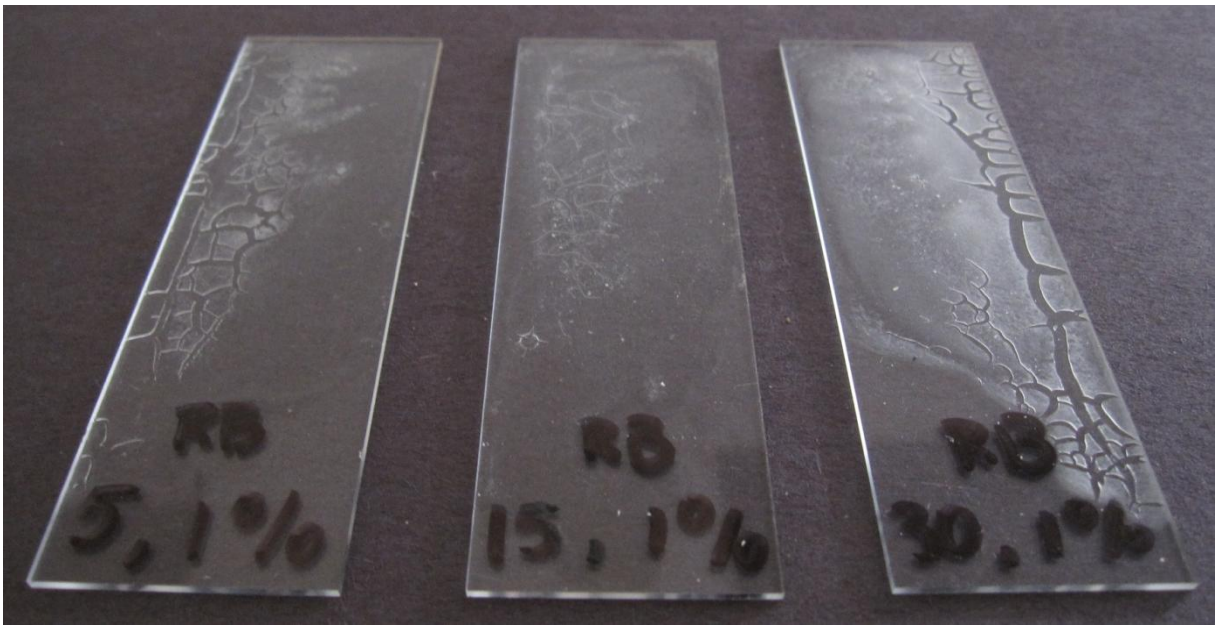

Figure D.1: 10% aerogel by weight to Nafion; 5, 15, and 30 minute powder (from left to right)

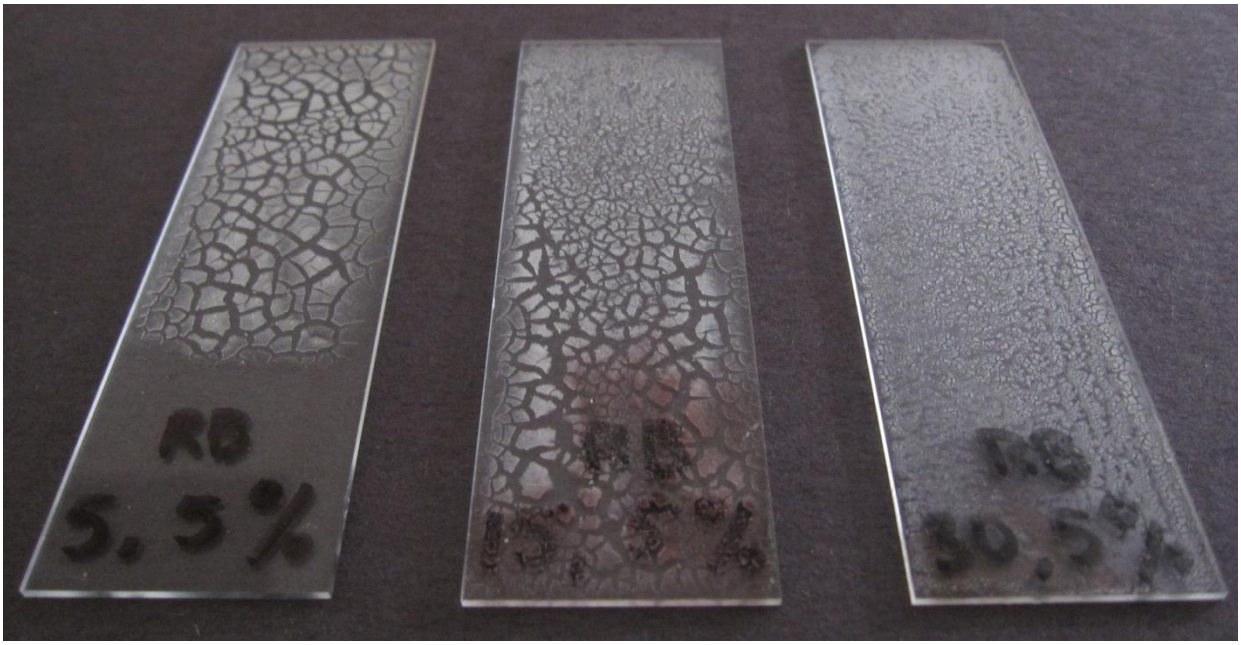

Figure D.2: 50% aerogel by weight to Nafion; 5, 15, and 30 minute powder (from left to right)

Appendix E: Contact Angle Measurements on Films in Appendix D

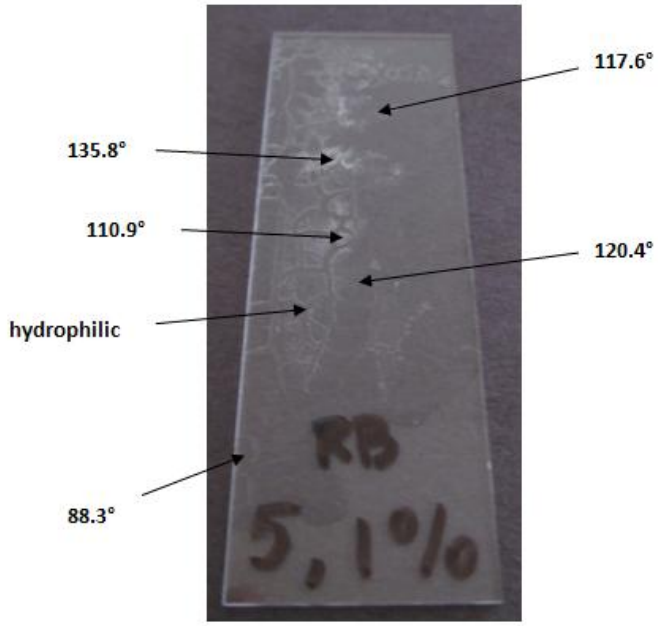

Figure E.1: 10% aerogel by weight to Nafion; 5 minute powder

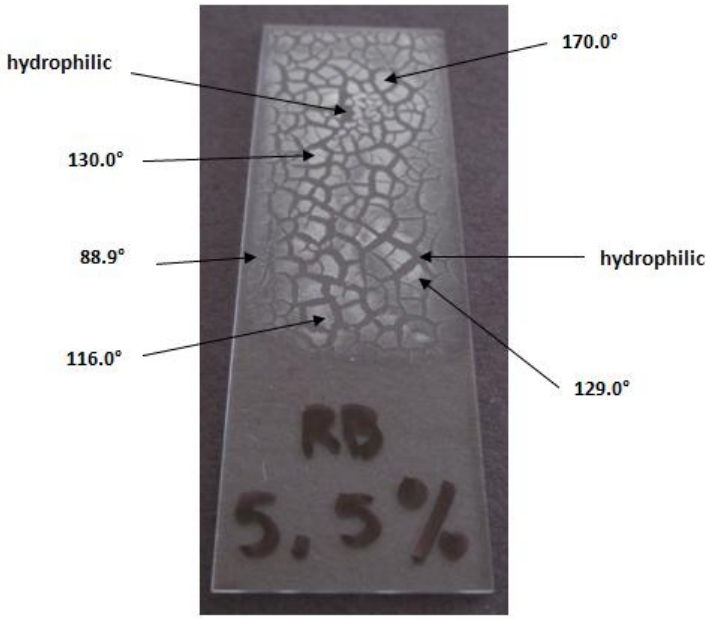

Figure E.2: 50% aerogel by weight to Nafion; 5 minute powder

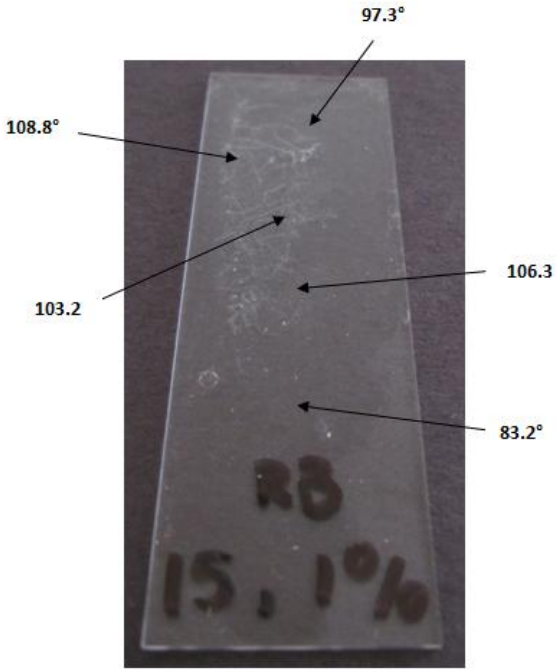

Figure E.3: 10% aerogel by weight to Nafion; 15 minute powder

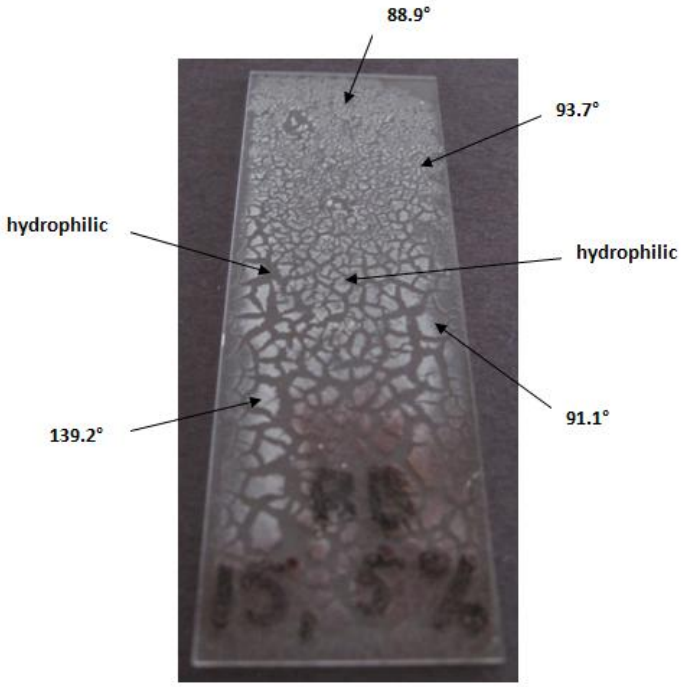

Figure E.4: 50% aerogel by weight to Nafion; 15 minute powder

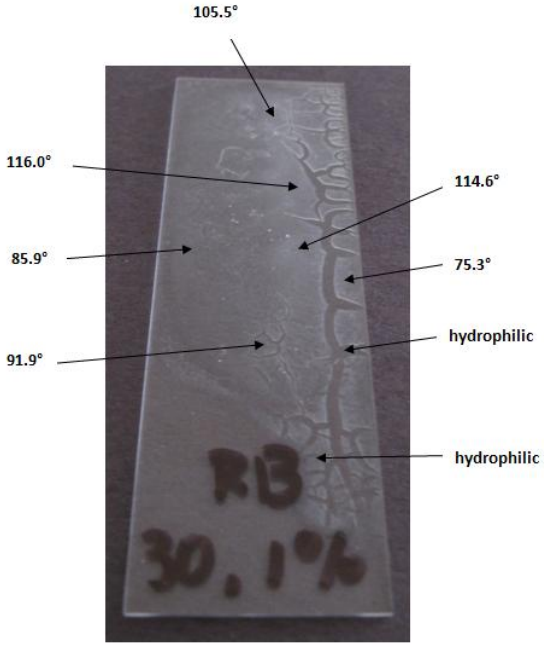

Figure E.5: 10% aerogel by weight to Nafion; 30 minute powder

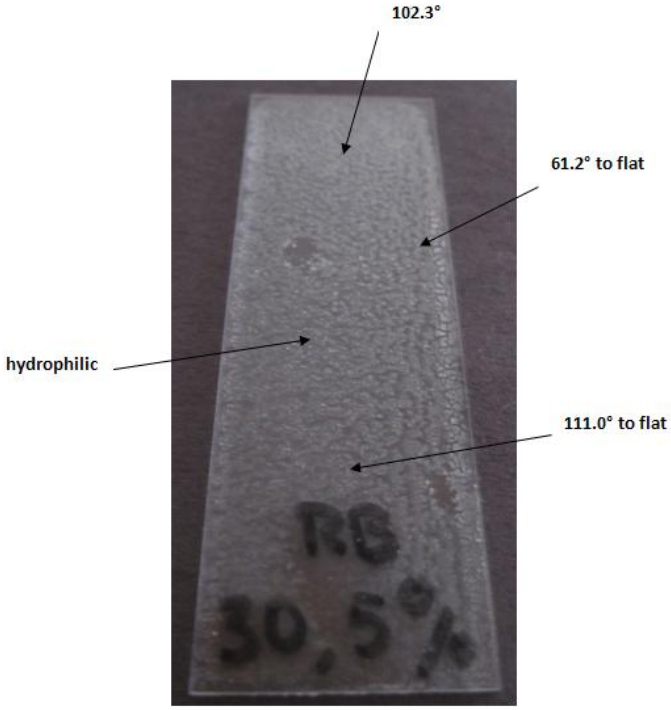

Figure E.6: 50% aerogel by weight to Nafion; 30 minute powder

Appendix F: 10% and 50% Aerogel Dried Sealed in Tupperware

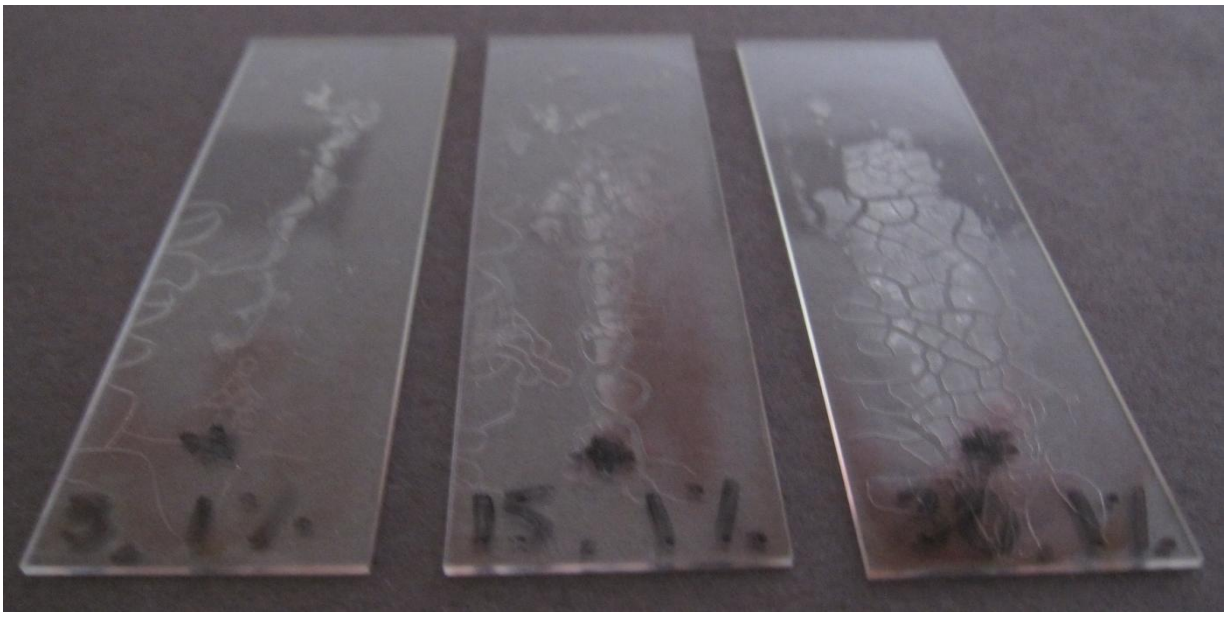

Figure F.1: 10% aerogel by weight to Nafion; 5, 15, and 30 minute powder (from left to right)

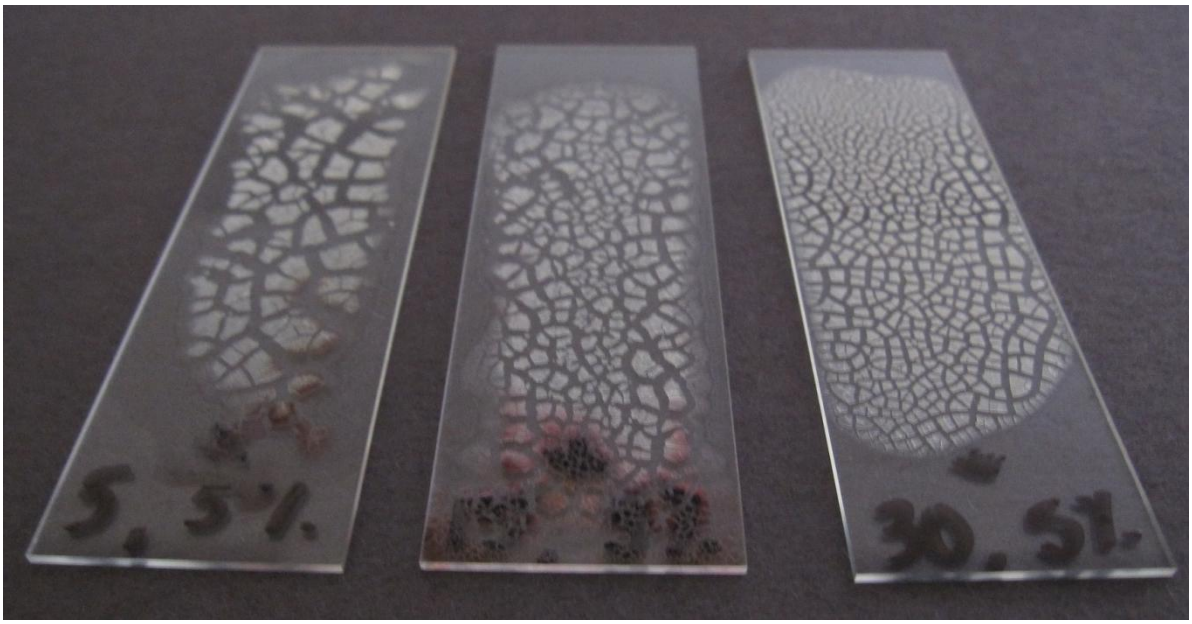

Figure F.2: 50% aerogel by weight to Nafion; 5, 15, and 30 minute powder (from left to right)

Appendix G: 5% Aerogel by Weight to Nafion

Figure G.1: 5% aerogel by weight to Nafion; 30 minute powder

Appendix H: High Aerogel Concentration Films

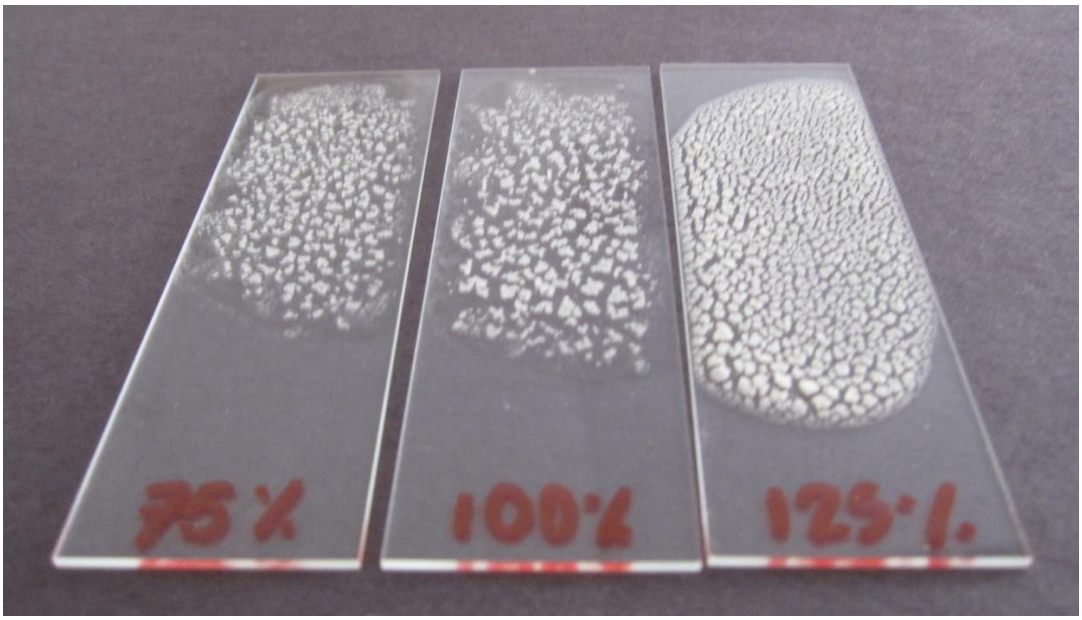

Figure H.1: 75, 100, and 125% aerogel by weight to Nafion (from left to right); 30 minute powder

Appendix I: 250% Aerogel Film

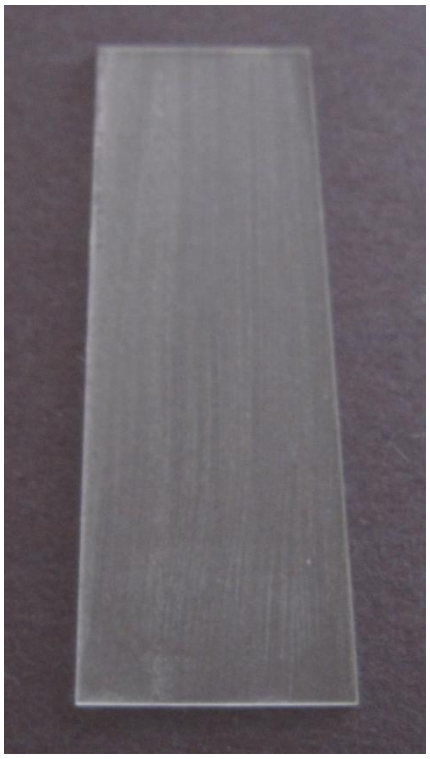

Figure I.1: 250% aerogel by weight to Nafion; 30 minute powder

Appendix J: Comparing Nafion Solutions

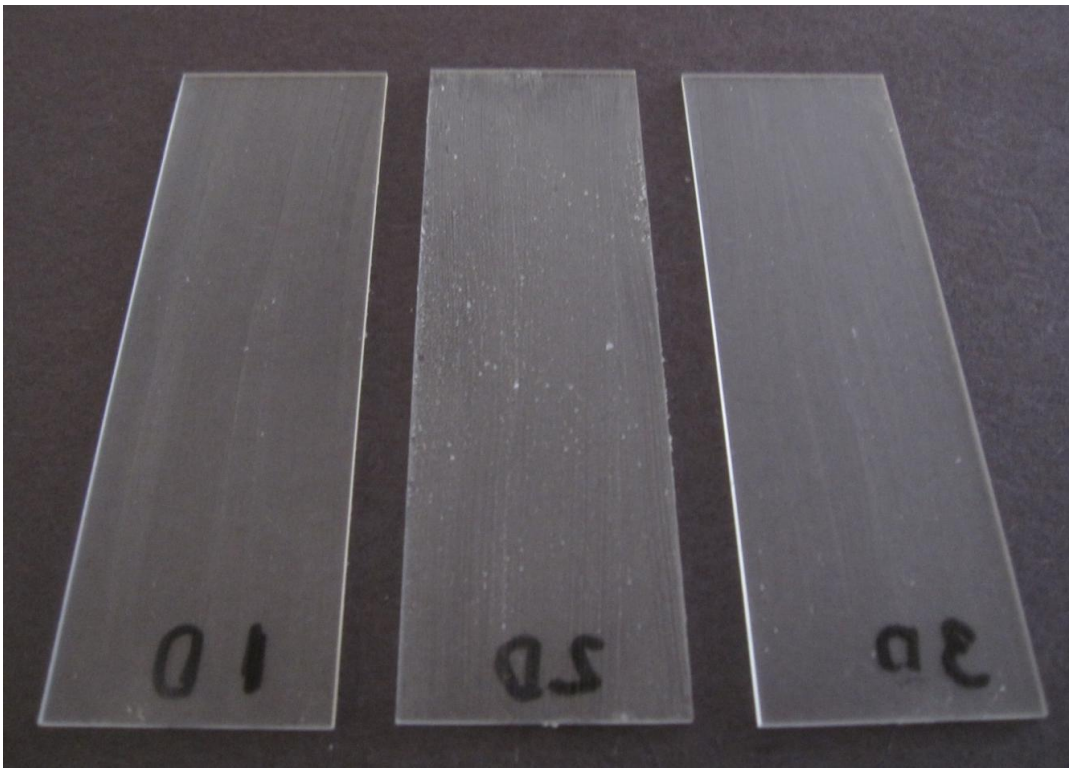

Figure J.1: 250% aerogel by weight to Nafion; 20 minute powder
(from left to right: Films 1, 2, and 3)

Appendix K: Procedure for Final Film Fabrication

1. Fabricate SH aerogel (50:50 TMOS to MTMS)
2. Crush aerogel for 20 minutes with a mortar and pestle using propanol as a solvent (add enough propanol to keep the powder moist during grinding; amount will vary based on the volume of aerogel being crushed)
3. Dry aerogel powder in a petridish (lid slightly uncovered) for 24 hours in the hood
4. Add appropriate amounts of superhydrophobic aerogel (0.218 g), Nafion (5 wt.% Nafion, 15 – 20 wt.% water) (2 ml), and propanol (4 ml) into a glass vial
5. Sonicate the solution for 5 minutes
6. Prepare the surface to be coated by dip coating (rinsing) in propanol
7. Paint a single coat of the solution onto the surface with a paintbrush (try to make the coating as uniform as possible)
8. Dry the surface in the hood for 24 hours before testing

Figure K.1: Final film

Appendix L: Film Fabricated with EG – 8

Table L.1: 4.571 ml recipe to fabricate EG – 8

Chemical	Amount
MTMS	1.063 ml
TMOS	1.063 ml
Methanol	0.875 ml
Water	0.90 ml
Ammonia	0.67 ml

NOTE: This recipe is the same recipe I use, but has twice the amount of catalyst.

Table L.2: Recipe used to fabricate the film using EG – 8

Chemical	Amount
Nafion	0.5 ml
Propanol	1 ml
Aerogel	0.0549 g

NOTE: I was limited by the amount of aerogel in the sample, so I had to make one-quarter of the usual recipe to replicate the final film using EG – 8. I believe that this had an effect on the film. This film cannot be directly compared to the other films for this reason.

Table L.3: Contact angle measurements of the film made using EG – 8

Contact Angle Measurements		
	Slide A	Slide B
average	129°	136°
st. dev	8°	12°
% st. dev	7%	9%

NOTE: Areas on both the slides were very hydrophobic (to a degree that drops could not be placed on the surface).

Appendix M: Procedure for Choosing Appropriate Ball

Careful consideration went into choosing the appropriate ball to use during this experiment. The most important parameters to satisfy were Reynolds number and coefficient of drag. Hollow balls seemed to be the best option; the density could be adjusted by replacing the air in the center of the ball with heavier mass. Racquetballs, practice rubber golf balls, and ping pong balls (varying sizes) were purchased (Figure M.1).

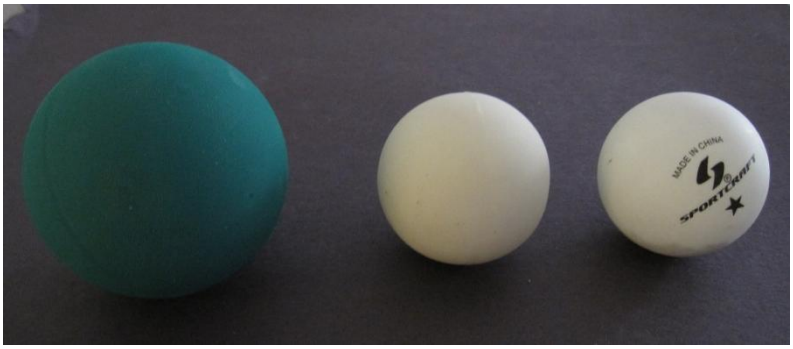

Figure M.1: Racquetball, practice rubber golf ball, ping pong ball (from left to right)

The density of each ball could be increased by inserting small steel balls (0.13 grams each) into the balls through a small hole (drilled out, and then sealed with silicone sealant). A range of densities that would be appropriate for testing were calculated for each type of ball. It was determined that to achieve laminar flows in our test apparatus the ideal coefficient of drag was 0.4. After preliminary testing, it was determined that the ping pong ball produced the most promising results. The ping pong ball also had the best surface to coat with the superhydrophobic aerogel coating (see Figure M.2 for the non-uniform coating on the practice rubber golf ball).

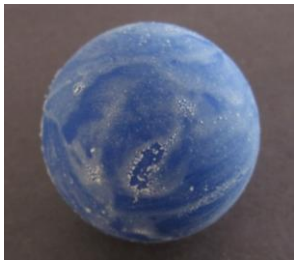

Figure M.2: Aerogel surface coating on practice rubber golf ball

Appendix N: Ping Pong Ball Testing Preparation

1. Drill a 0.120 inch diameter hole into the ping pong ball
2. Insert the appropriate amount of steel balls (0.13 grams each) into the ping pong ball until it weighs the desired amount
3. Seal the hole with IS808 General Purpose Silicone Rubber Adhesive Sealant; dry for 24 hours
4. Use a paintbrush to apply a single coat of aerogel film onto the ball; dry for 24 hours
5. Verify the weight of the ball before testing

Figure N.1: Coated ping pong ball

Appendix O: Data from Falling Ball Experiment

	Ball A - uncoated		
	mass (kg)	0.032779	
	time (s)	vel (m/s)	C_D
	3.5	0.051	3.2
	3.32	0.054	2.9
	3.78	0.047	3.7
	3.53	0.050	3.3
	3.59	0.050	3.4
	3.32	0.054	2.9
	3.5	0.051	3.2
	3.53	0.050	3.3
	3.57	0.050	3.3
	3.38	0.053	3.0
	3.59	0.050	3.4
	3.44	0.052	3.1
	3.47	0.051	3.2
	3.63	0.049	3.5
	3.72	0.048	3.6
	3.72	0.048	3.6
	3.78	0.047	3.7
	3.75	0.047	3.7
	3.69	0.048	3.6
	3.53	0.050	3.3
average	3.57		3.3
st. dev	0.14		
% st. dev	4%		
avg vel (cm/s)	4.98		
avg vel (m/s)	0.050		
avg Re	2018		
F_D	0.00537		

Table O.1: Ball A - uncoated

	Ball A - coated		
	mass (kg)	0.032794	
	time (s)	vel (m/s)	C_D
	3.88	0.046	3.7
	4.03	0.044	4.0
	3.91	0.045	3.7
	3.65	0.049	3.3
	3.57	0.050	3.1
	3.66	0.049	3.3
	3.81	0.047	3.6
	3.81	0.047	3.6
	3.65	0.049	3.3
	3.59	0.050	3.2
	3.47	0.051	2.9
	3.47	0.051	2.9
	3.90	0.046	3.7
	3.72	0.048	3.4
	3.60	0.049	3.2
	3.94	0.045	3.8
	3.44	0.052	2.9
	3.66	0.049	3.3
	3.88	0.046	3.7
	3.93	0.045	3.8
average	3.73		3.4
st. dev	0.18		
% st. dev	5%		
avg vel (cm/s)	4.77		
avg vel (m/s)	0.048		
avg Re	1930		
F_D	0.00501		

Table O.2: Ball A -coated

	Ball B - uncoated		
	mass (kg)	0.03303	
	time (s)	vel (m/s)	C_D
	2.93	0.061	3.7
	2.91	0.061	3.7
	2.75	0.065	3.3
	2.78	0.064	3.4
	2.79	0.064	3.4
	2.63	0.068	3.0
	2.6	0.068	2.9
	2.56	0.069	2.8
	2.43	0.073	2.6
	2.53	0.070	2.8
	2.63	0.068	3.0
	2.94	0.060	3.8
	2.62	0.068	3.0
	2.56	0.069	2.8
	2.46	0.072	2.6
	2.84	0.063	3.5
	2.62	0.068	3.0
	2.47	0.072	2.7
	2.88	0.062	3.6
	2.66	0.067	3.1
average	2.68		3.1
st. dev	0.16		
% st. dev	6%		
avg vel (cm/s)	6.64		
avg vel (m/s)	0.066		
avg Re	2681		
F_D	0.00886		

Table O.3: Ball B - uncoated

	Ball B - coated		
	mass (kg)	0.033048	
	time (s)	vel (m/s)	C_D
	3.25	0.055	4.2
	2.84	0.063	3.2
	3.09	0.058	3.8
	3.06	0.058	3.7
	3.13	0.057	3.9
	3.16	0.056	3.9
	3.19	0.056	4.0
	2.69	0.066	2.8
	3.10	0.057	3.8
	3.06	0.058	3.7
	2.93	0.061	3.4
	2.59	0.069	2.6
	2.97	0.060	3.5
	2.90	0.061	3.3
	2.71	0.066	2.9
	2.91	0.061	3.3
	3.00	0.059	3.5
	2.97	0.060	3.5
	3.06	0.058	3.7
	3.00	0.059	3.5
average	2.98		3.5
st. dev	0.17		
% st. dev	6%		
avg vel (cm/s)	5.97		
avg vel (m/s)	0.060		
avg Re	2411		
F_D	0.00803		

Table O.4: Ball B - coated

	Ball C - uncoated		
	mass (kg)	0.033223	
	time (s)	vel (m/s)	C_D
	2.38	0.075	3.2
	2.22	0.080	2.8
	2.26	0.079	2.9
	2.25	0.079	2.9
	2.47	0.072	3.5
	2.13	0.083	2.6
	2.5	0.071	3.6
	2.47	0.072	3.5
	2.35	0.076	3.1
	2.41	0.074	3.3
	2.44	0.073	3.4
	2.41	0.074	3.3
	2.22	0.080	2.8
	2.41	0.074	3.3
	2.57	0.069	3.8
	2.46	0.072	3.4
	2.47	0.072	3.5
	2.41	0.074	3.3
	2.41	0.074	3.3
	2.25	0.079	2.9
average	2.37		3.2
st. dev	0.12		
% st. dev	5%		
avg vel (cm/s)	7.49		
avg vel (m/s)	0.075		
avg Re	3018		
F_D	0.01153		

Table O.5: Ball C - uncoated

	Ball C - coated		
	mass (kg)	0.033237	
	time (s)	vel (m/s)	C_D
	2.72	0.065	3.9
	2.50	0.071	3.3
	2.72	0.065	3.9
	2.40	0.074	3.0
	2.75	0.065	4.0
	2.28	0.078	2.8
	2.66	0.067	3.7
	2.72	0.065	3.9
	2.71	0.066	3.9
	2.71	0.066	3.9
	2.50	0.071	3.3
	2.56	0.069	3.5
	2.53	0.070	3.4
	2.60	0.068	3.6
	2.28	0.078	2.8
	2.31	0.077	2.8
	2.53	0.070	3.4
	2.16	0.082	2.5
	2.53	0.070	3.4
	2.72	0.065	3.9
average	2.54		3.4
st. dev	0.18		
% st. dev	7%		
avg vel (cm/s)	6.99		
avg vel (m/s)	0.070		
avg Re	2816		
F_D	0.01074		

Table O.6: Ball C - coated

	Ball D - uncoated		
	mass (kg)	0.033418	
	time (s)	vel (m/s)	C_D
	2.34	0.076	3.1
	2.28	0.078	2.9
	2.22	0.080	2.8
	2.28	0.078	2.9
	2.4	0.074	3.2
	2.43	0.073	3.3
	2.34	0.076	3.1
	2.38	0.075	3.2
	2.32	0.077	3.0
	2.34	0.076	3.1
	2.19	0.081	2.7
	2.31	0.077	3.0
	2.31	0.077	3.0
	2.28	0.078	2.9
	2.28	0.078	2.9
	2.37	0.075	3.2
	2.25	0.079	2.9
	2.21	0.080	2.7
	2.28	0.078	2.9
	2.37	0.075	3.2
average	2.31		3.0
st. dev	0.06		
% st. dev	3%		
avg vel (cm/s)	7.70		
avg vel (m/s)	0.077		
avg Re	3118		
F_D	0.01153		

Table O.7: Ball D - uncoated

	Ball D - coated		
	mass (kg)	0.033462	
	time (s)	vel (m/s)	C_D
	2.81	0.063	4.2
	2.44	0.073	3.1
	2.63	0.068	3.7
	2.53	0.070	3.4
	2.81	0.063	4.2
	2.31	0.077	2.8
	2.78	0.064	4.1
	2.37	0.075	3.0
	2.43	0.073	3.1
	2.57	0.069	3.5
	2.62	0.068	3.6
	2.50	0.071	3.3
	2.37	0.075	3.0
	2.59	0.069	3.5
	2.41	0.074	3.1
	2.50	0.071	3.3
	2.53	0.070	3.4
	2.71	0.066	3.9
	2.66	0.067	3.7
	2.53	0.070	3.4
average	2.56		3.5
st. dev	0.15		
% st. dev	6%		
avg vel (cm/s)	6.96		
avg vel (m/s)	0.070		
avg Re	2818		
F_D	0.01081		

Table O.8: Ball D - coated

Appendix P: Spindle Specifications

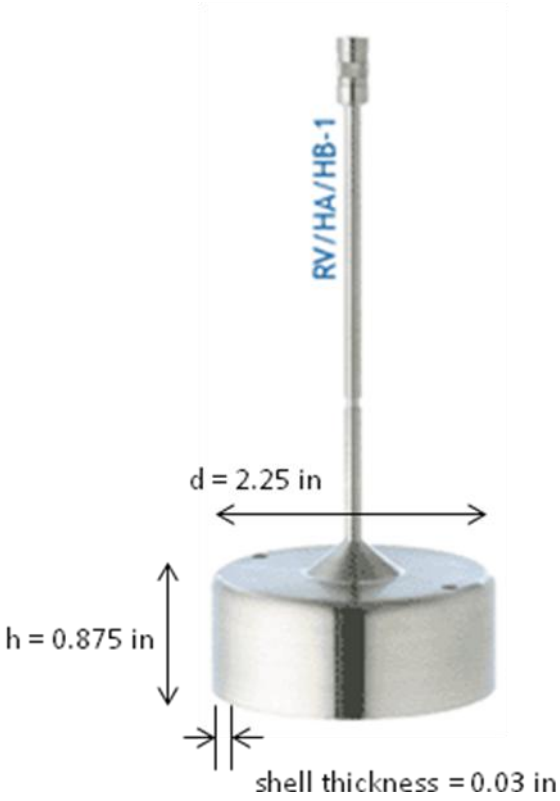

Figure P.1: Spindle S01

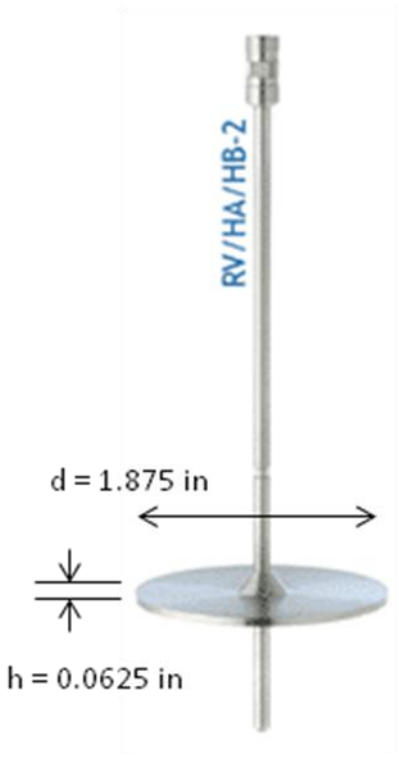

Figure P.2: Spindle S02

Material: #302 Stainless Steel

Appendix Q: Final Procedure for Rotational Viscometer Experiment

1. If the spindle is going to be tested uncoated, clean it with propanol using a KimWipe and allow to dry overnight in the hood; if the spindle is going to be tested with a coating, apply a thin coating of aerogel film on the spindle using a paintbrush (see Appendix for instructions on making films) and allow to dry overnight in the hood
2. Fill a 1000 ml beaker with room temperature water (use a thermometer to record the temperature of the water)
3. Mount spindle on the viscometer and submerge the spindle up to the notch on the shaft (make sure there are no air bubbles trapped under the spindle)
4. Turn the viscometer on and select the type of spindle being used
5. Set the rotational speed to 30 rpm and turn on the motor
6. Using a stopwatch, allow the viscometer to stabilize for one minute
7. Manually record the percent torque every ten seconds for ten readings
8. Increase the rotational speed to 50 rpm, allow the viscometer to stabilize for one minute, manually record the percent torque every ten seconds for ten readings
9. Increase the rotational speed to 60 rpm, allow the viscometer to stabilize for one minute, manually record the percent torque every ten seconds for ten readings
10. After all three rotational speeds are recorded, turn the motor off, completing trial 1
11. Repeat the procedure (beginning from Step 3) for a total of 4 trials
12. Use a KimWipe and propanol to remove the coating from the spindle at the end of the experiment

Appendix R: Rotational Viscometer Results

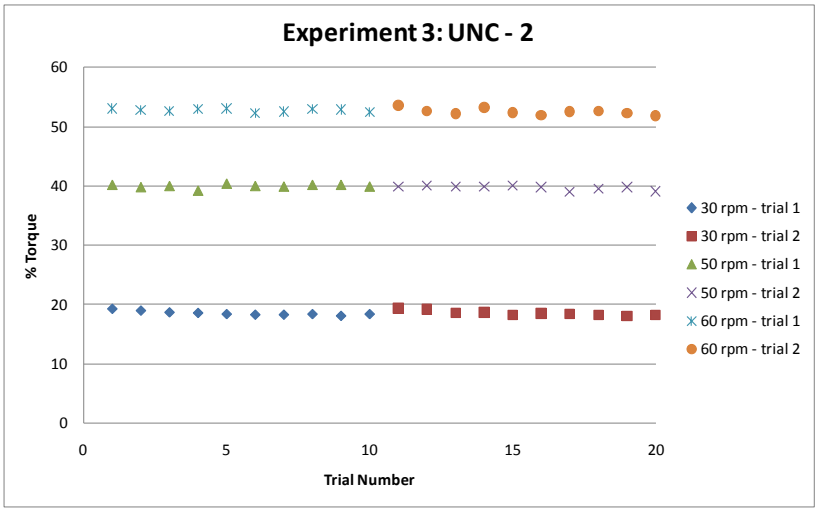

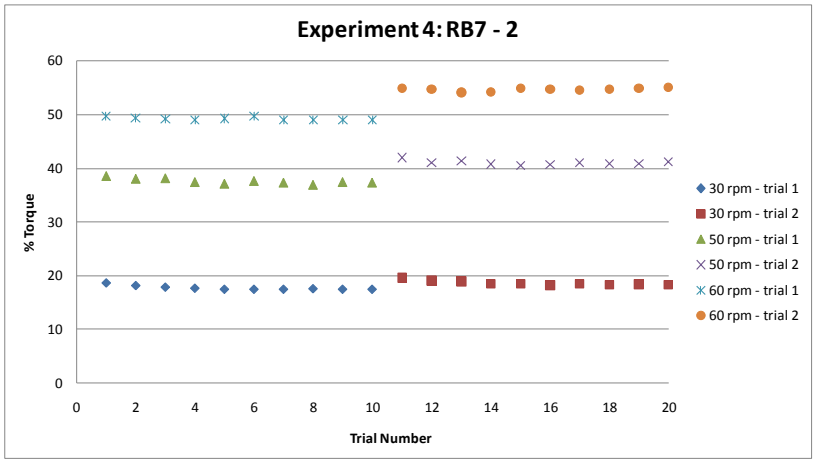

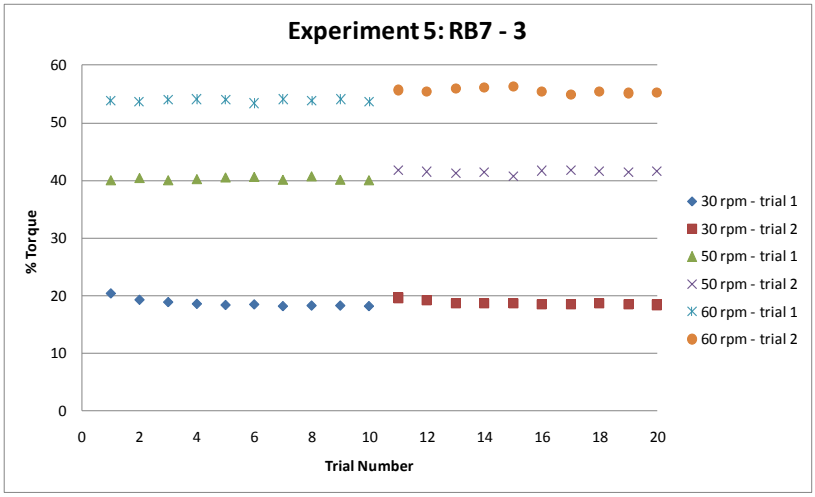

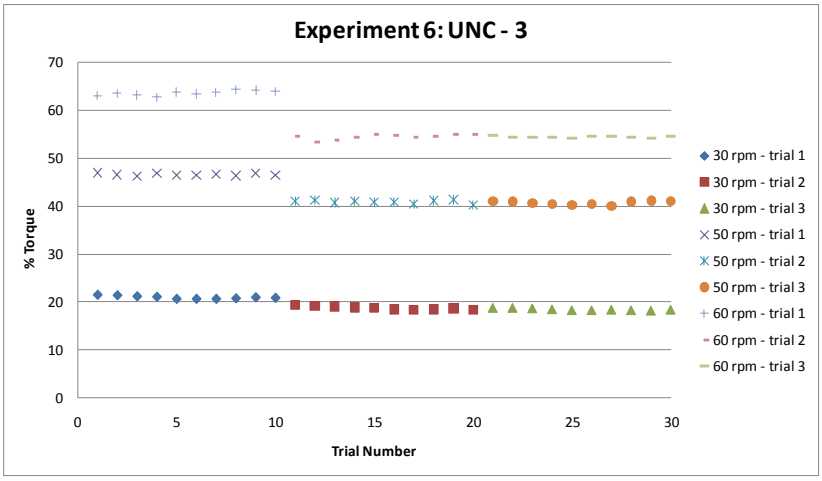
Experiment 6: UNC - 3
% Torque
Trial Number
0
10
20
30
40
50
60
70
0
5
10
15
20
25
30
30 rpm - trial 1
30 rpm - trial 2
30 rpm - trial 3
50 rpm - trial 1
50 rpm - trial 2
50 rpm - trial 3
60 rpm - trial 1
60 rpm - trial 2
60 rpm - trial 3

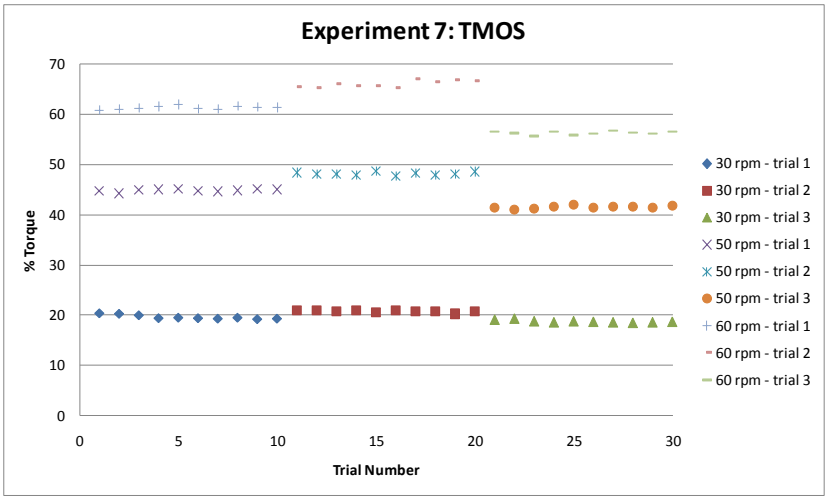
Experiment 7: TMOS
% Torque
Trial Number
0
10
20
30
40
50
60
70
0
5
10
15
20
25
30
30 rpm - trial 1
30 rpm - trial 2
30 rpm - trial 3
50 rpm - trial 1
50 rpm - trial 2
50 rpm - trial 3
60 rpm - trial 1
60 rpm - trial 2
60 rpm - trial 3

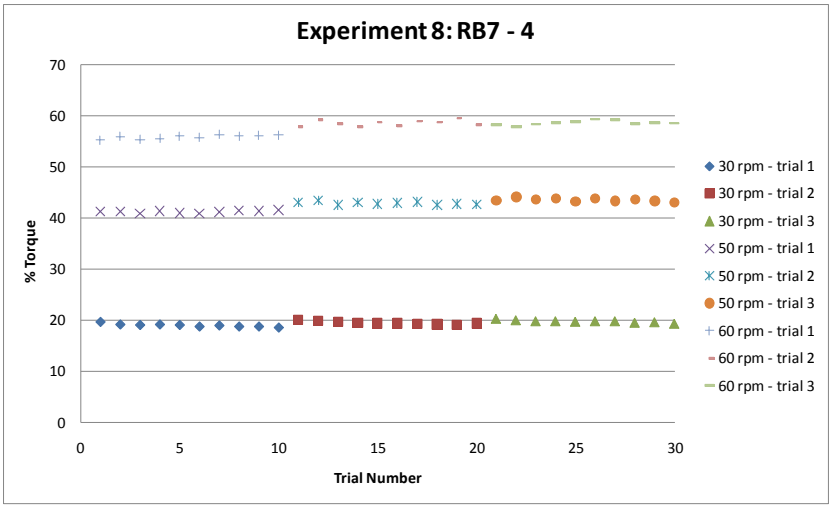
Experiment 8: RB7 - 4
% Torque
Trial Number
0
10
20
30
40
50
60
70
0
5
10
15
20
25
30
30 rpm - trial 1
30 rpm - trial 2
30 rpm - trial 3
50 rpm - trial 1
50 rpm - trial 2
50 rpm - trial 3
60 rpm - trial 1
60 rpm - trial 2
60 rpm - trial 3

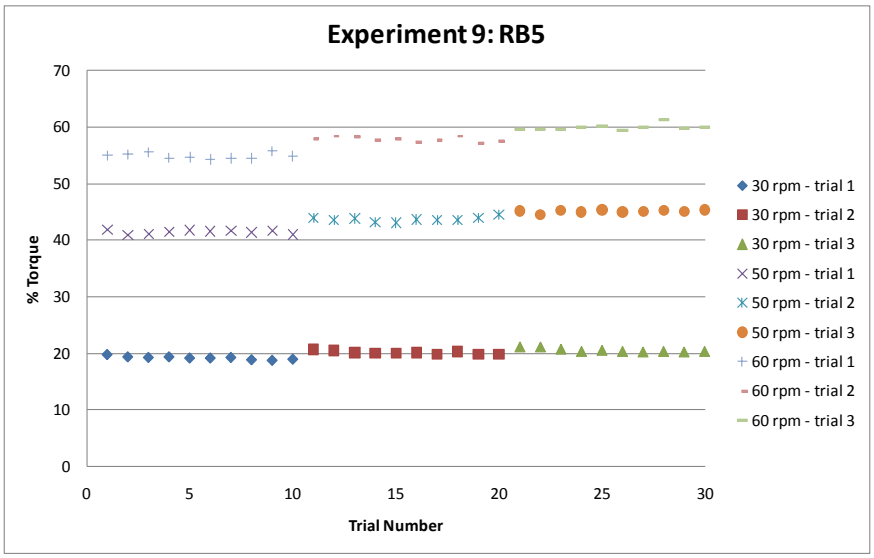
Experiment 9: RB5
% Torque
Trial Number
0
10
20
30
40
50
60
70
0
5
10
15
20
25
30
30 rpm - trial 1
30 rpm - trial 2
30 rpm - trial 3
50 rpm - trial 1
50 rpm - trial 2
50 rpm - trial 3
60 rpm - trial 1
60 rpm - trial 2
60 rpm - trial 3

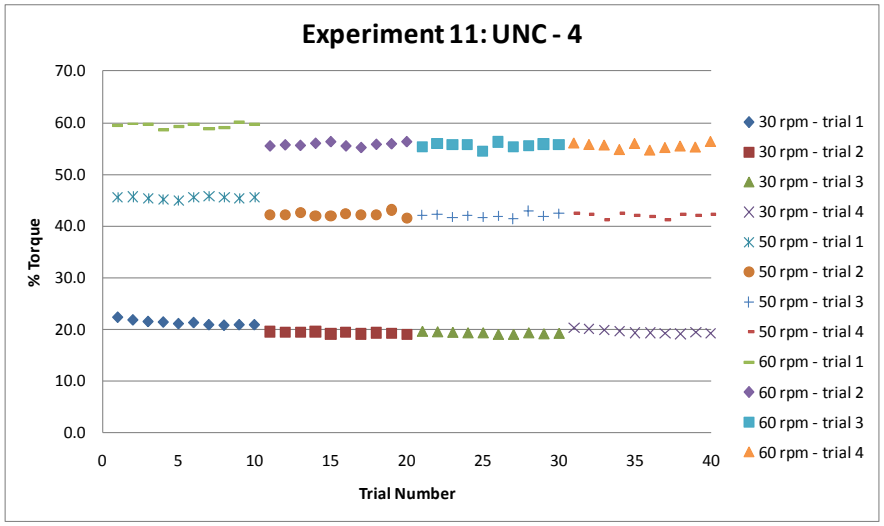
Experiment 11: UNC - 4
% Torque
Trial Number
0.0
10.0
20.0
30.0
40.0
50.0
60.0
70.0
0
5
10
15
20
25
30
35
40
30 rpm - trial 1
30 rpm - trial 2
30 rpm - trial 3
30 rpm - trial 4
50 rpm - trial 1
50 rpm - trial 2
50 rpm - trial 3
50 rpm - trial 4
60 rpm - trial 1
60 rpm - trial 2
60 rpm - trial 3
60 rpm - trial 4

Appendix S: Percent Torque Data – Spindle S01

The tables in this appendix show percent torque values that were manually recorded from the digital display on the rotational viscometer. During each experiment, different rotational speeds were tested. At each speed (and for each individual trial) the average percent torque and standard deviation in percent torque were calculated. Table 4.2 summarizes the conditions under which each experiment was conducted.

	Experiment 1: UNC - 1					
	5 rpm	**10 rpm**	**20 rpm**	**30 rpm**	**50 rpm**	**60 rpm**
	2.4	4.5	11.1	19.4	42.8	58.4
	2.4	4.3	10.8	19.2	43	57.8
	2.4	4.3	10.9	19.3	42.7	58.7
	2.4	4.3	10.9	19.1	43.2	58.3
	2.5	4.2	10.7	19.3	43.3	58
	2.4	4.2	10.4	19.2	42.8	58.7
	2.5	4.2	10.4	19.4	42.6	58.5
	2.4	4.1	10.5	19.2	43.6	57.8
	2.4	4.2	10.6	19.2	43.3	58.7
	2.4	4.2	10.8	19.3	43.1	57.7
avg	**2.42**	**4.25**	**10.71**	**19.26**	**43.04**	**58.26**
st dev	**0.04**	**0.11**	**0.23**	**0.10**	**0.32**	**0.40**

	Experiment 2: RB7 - 1		
	30 rpm	**50 rpm**	**60 rpm**
	18	39	52.3
	17.9	38.7	52.2
	17.9	38.6	52
	17.8	39.1	52.2
	17.8	38.2	51.5
	18.1	38.7	51.2
	17.9	38.7	52.3
	17.9	38.5	52.8
	17.9	39.7	52.2
	17.8	38.6	51.1
avg	**17.9**	**38.78**	**51.98**
st dev	**0.09**	**0.41**	**0.54**

	Experiment 3: UNC - 2					
	trial 1			trial 2		
	30 rpm	50 rpm	60 rpm	30 rpm	50 rpm	60 rpm
	19.3	40.2	53.1	19.4	39.9	53.6
	19	39.8	52.8	19.2	40.1	52.7
	18.7	40	52.7	18.6	39.9	52.2
	18.6	39.2	53	18.7	39.9	53.3
	18.4	40.4	53.1	18.3	40.1	52.4
	18.3	40	52.3	18.5	39.8	52
	18.3	39.9	52.6	18.4	39	52.6
	18.4	40.2	53	18.2	39.6	52.7
	18.1	40.2	52.9	18.1	39.8	52.3
	18.4	39.9	52.5	18.2	39.1	51.9
avg	**18.55**	**39.98**	**52.8**	**18.56**	**39.72**	**52.57**
st dev	**0.36**	**0.33**	**0.27**	**0.44**	**0.38**	**0.54**

	Experiment 4: RB7 - 2					
	trial 1			trial 2		
	30 rpm	50 rpm	60 rpm	30 rpm	50 rpm	60 rpm
	18.7	38.6	49.8	19.6	42	55
	18.2	38.1	49.4	19.1	41.1	54.8
	17.9	38.2	49.2	18.9	41.4	54.2
	17.7	37.5	49.1	18.5	40.8	54.3
	17.5	37.2	49.3	18.5	40.5	55
	17.5	37.7	49.8	18.2	40.7	54.8
	17.5	37.4	49.1	18.5	41.1	54.6
	17.6	37	49	18.3	40.9	54.8
	17.5	37.5	49.1	18.4	40.9	55
	17.5	37.4	49	18.3	41.2	55.1
avg	**17.76**	**37.66**	**49.28**	**18.63**	**41.06**	**54.76**
st dev	**0.40**	**0.49**	**0.30**	**0.44**	**0.42**	**0.31**

	Experiment 5: RB7 - 3					
	trial 1			trial 2		
	30 rpm	50 rpm	60 rpm	30 rpm	50 rpm	60 rpm
	20.4	40	53.9	19.6	41.8	55.7
	19.3	40.4	53.7	19.2	41.5	55.5
	18.9	40	54	18.7	41.2	56
	18.6	40.2	54.1	18.7	41.4	56.1
	18.4	40.5	54	18.6	40.7	56.3
	18.5	40.6	53.4	18.5	41.7	55.5
	18.2	40.1	54.1	18.5	41.8	54.9
	18.3	40.7	53.9	18.6	41.6	55.4
	18.3	40.1	54.1	18.5	41.4	55.2
	18.2	40	53.7	18.4	41.6	55.3
avg	**18.71**	**40.26**	**53.89**	**18.73**	**41.47**	**55.59**
st dev	**0.69**	**0.27**	**0.23**	**0.38**	**0.33**	**0.44**

	Experiment 6: UNC - 3								
	trial 1			trial 2			trial 3		
	30 rpm	50 rpm	60 rpm	30 rpm	50 rpm	60 rpm	30 rpm	50 rpm	60 rpm
	21.5	47	63.1	19.4	41.1	54.7	18.8	41.1	54.8
	21.4	46.6	63.6	19.2	41.3	53.5	18.8	41	54.5
	21.2	46.3	63.3	19.1	40.8	53.8	18.7	40.7	54.4
	21.1	46.9	62.8	18.9	41.1	54.5	18.5	40.4	54.4
	20.7	46.5	63.9	18.8	40.9	55.1	18.3	40.2	54.2
	20.7	46.5	63.5	18.5	40.9	54.8	18.3	40.5	54.6
	20.7	46.7	63.8	18.3	40.5	54.5	18.4	40.1	54.7
	20.8	46.4	64.4	18.5	41.2	54.7	18.3	41	54.5
	21	46.9	64.3	18.7	41.4	55	18.2	41.2	54.3
	20.9	46.5	64	18.4	40.2	55.1	18.4	41.1	54.7
avg	**21.00**	**46.63**	**63.67**	**18.78**	**40.94**	**54.57**	**18.47**	**40.73**	**54.51**
st dev	**0.29**	**0.24**	**0.51**	**0.37**	**0.37**	**0.54**	**0.22**	**0.41**	**0.19**

	Experiment 7: TMOS								
	trial 1			trial 2			trial 3		
	30 rpm	50 rpm	60 rpm	30 rpm	50 rpm	60 rpm	30 rpm	50 rpm	60 rpm
	20.4	44.8	60.9	21	48.4	65.5	19.1	41.5	56.6
	20.3	44.3	61.1	21	48.1	65.4	19.3	41	56.3
	20	45	61.3	20.7	48.2	66.1	18.8	41.2	55.7
	19.4	45.1	61.6	21	48	65.7	18.6	41.7	56.6
	19.5	45.2	62	20.6	48.7	65.7	18.8	42	55.9
	19.4	44.8	61.2	20.9	47.8	65.4	18.7	41.4	56.2
	19.3	44.7	61.1	20.7	48.3	67.1	18.6	41.7	56.8
	19.5	44.9	61.7	20.8	47.9	66.5	18.5	41.6	56.4
	19.2	45.2	61.5	20.3	48.1	66.9	18.6	41.5	56.2
	19.3	45.1	61.4	20.8	48.6	66.7	18.7	41.8	56.6
avg	**19.63**	**44.91**	**61.38**	**20.78**	**48.21**	**66.1**	**18.77**	**41.54**	**56.33**
st dev	**0.44**	**0.28**	**0.33**	**0.22**	**0.29**	**0.65**	**0.25**	**0.29**	**0.34**

	Experiment 8: RB7 - 4								
	trial 1			trial 2			trial 3		
	30 rpm	50 rpm	60 rpm	30 rpm	50 rpm	60 rpm	30 rpm	50 rpm	60 rpm
	19.7	41.3	55.3	20.1	43.1	58	20.3	43.5	58.3
	19.2	41.3	56	19.9	43.5	59.3	20	44.2	58
	19.1	40.9	55.4	19.7	42.6	58.5	19.8	43.7	58.4
	19.2	41.4	55.6	19.5	43.1	58	19.8	43.9	58.7
	19.1	41	56.1	19.4	42.8	58.8	19.7	43.3	58.9
	18.8	40.9	55.8	19.4	43	58.1	19.8	43.9	59.4
	19	41.2	56.4	19.3	43.2	59	19.8	43.4	59.3
	18.8	41.5	56.1	19.2	42.6	58.8	19.5	43.7	58.5
	18.8	41.4	56.2	19.1	42.8	59.6	19.6	43.4	58.7
	18.6	41.6	56.3	19.4	42.7	58.3	19.3	43.1	58.6
avg	**19.03**	**41.25**	**55.92**	**19.5**	**42.94**	**58.64**	**19.76**	**43.61**	**58.68**
st dev	**0.31**	**0.25**	**0.38**	**0.31**	**0.29**	**0.56**	**0.27**	**0.33**	**0.43**

	Experiment 9: RB5								
	trial 1			trial 2			trial 3		
	30 rpm	50 rpm	60 rpm	30 rpm	50 rpm	60 rpm	30 rpm	50 rpm	60 rpm
	19.8	41.9	55	20.7	44	57.9	21.1	45.2	59.6
	19.4	40.9	55.2	20.5	43.6	58.4	21.1	44.5	59.6
	19.3	41.1	55.6	20.1	43.9	58.3	20.7	45.3	59.6
	19.4	41.5	54.6	20	43.2	57.8	20.3	45	60.1
	19.2	41.8	54.7	20	43.1	58	20.5	45.4	60.2
	19.2	41.6	54.3	20.1	43.7	57.4	20.3	45	59.5
	19.3	41.7	54.5	19.9	43.6	57.7	20.2	45.1	60
	18.9	41.4	54.5	20.3	43.6	58.4	20.3	45.3	61.3
	18.8	41.7	55.8	19.8	44	57.1	20.2	45.1	59.8
	19	41	54.9	19.8	44.5	57.5	20.3	45.4	60
avg	**19.23**	**41.46**	**54.91**	**20.12**	**43.72**	**57.85**	**20.5**	**45.13**	**59.97**
st dev	**0.29**	**0.35**	**0.50**	**0.30**	**0.41**	**0.44**	**0.35**	**0.27**	**0.53**

	Experiment 10: RB7 - 5											
	trial 1			trial 2			trial 3			trial 4		
	30 rpm	50 rpm	60 rpm	30 rpm	50 rpm	60 rpm	30 rpm	50 rpm	60 rpm	30 rpm	50 rpm	60 rpm
	19.9	42.0	57.3	19.6	42.3	56.1	19.5	42.2	56.7	20.3	42.3	56.7
	19.8	42.4	56.9	19.5	42.7	56.2	19.8	42.1	55.5	20.1	43.0	57.0
	19.6	42.1	56.9	19.3	42.8	55.5	19.2	42.3	55.6	19.8	42.6	56.8
	19.5	42.6	58.0	19.5	42.3	55.3	19.1	42.0	56.6	19.6	42.5	57.1
	19.4	42.3	56.6	19.3	42.2	56.1	19.2	42.6	56.4	19.3	42.7	56.4
	19.4	42.4	57.2	19.1	42.1	56.0	19.0	42.2	56.0	19.3	42.4	57.1
	19.2	41.9	57.3	19.2	42.2	56.0	19.1	41.8	56.3	19.2	42.3	56.3
	19.0	42.4	57.1	19.0	42.4	56.1	19.0	42.2	55.9	19.1	42.6	56.3
	19.2	41.5	56.3	19.4	41.3	55.4	19.1	41.9	56.5	19.4	42.8	56.9
	19.1	42.3	57.7	19.1	41.6	56.2	19.0	42.9	56.0	19.2	43.1	56.7
avg	**19.41**	**42.19**	**57.13**	**19.3**	**42.19**	**55.89**	**19.2**	**42.22**	**56.15**	**19.53**	**42.63**	**56.73**
st dev	**0.30**	**0.32**	**0.50**	**0.20**	**0.45**	**0.35**	**0.26**	**0.33**	**0.41**	**0.41**	**0.28**	**0.31**

	Experiment 11: UNC - 4											
	trial 1			trial 2			trial 3			trial 4		
	30 rpm	50 rpm	60 rpm	30 rpm	50 rpm	60 rpm	30 rpm	50 rpm	60 rpm	30 rpm	50 rpm	60 rpm
	22.3	45.6	59.5	19.5	42.2	55.5	19.6	42.1	55.4	19.8	42.4	56.1
	21.8	45.7	59.8	19.4	42.1	55.7	19.5	42.2	56.0	19.7	42.3	55.8
	21.5	45.4	59.7	19.4	42.6	55.6	19.4	41.7	55.7	19.5	41.2	55.7
	21.4	45.1	58.7	19.5	41.9	56.0	19.3	42.0	55.8	19.4	42.5	54.8
	21.1	44.9	59.2	19.1	42.0	56.3	19.3	41.7	54.5	19.4	42.0	56.0
	21.3	45.6	59.6	19.4	42.4	55.5	19.0	41.9	56.3	19.4	41.9	54.7
	20.9	45.8	58.8	19.1	42.1	55.2	19.0	41.4	55.3	19.3	41.2	55.2
	20.8	45.5	59.1	19.3	42.1	55.8	19.3	42.9	55.6	19.5	42.2	55.5
	20.9	45.4	60.1	19.2	43.1	55.9	19.1	41.9	55.9	19.3	42.0	55.3
	20.9	45.6	59.7	19.0	41.5	56.3	19.2	42.4	55.8	19.1	42.3	56.4
avg	**21.29**	**45.46**	**59.42**	**19.29**	**42.2**	**55.78**	**19.27**	**42.02**	**55.63**	**19.44**	**42**	**55.55**
st dev	**0.48**	**0.28**	**0.45**	**0.18**	**0.43**	**0.36**	**0.20**	**0.42**	**0.49**	**0.20**	**0.46**	**0.56**

Appendix T: PIV Test Piece Preparation

1. Clean the surface of the test pieces with a KimWipe and propanol and allow to dry overnight in the hood. This should be done for both uncoated and coated test pieces
2. If the test piece will not be coated, it is ready for testing
3. If the test piece is going to be coated, evenly apply a thin coating of aerogel film to the surface of the test piece using a paintbrush (see Appendix for recipe and procedure to make films) and allow to dry overnight in the hood
4. Once the coating on the test piece is dry it is ready for testing

Appendix U: Experimental Procedure for PIV Testing

1. Prepare the test pieces appropriately for testing
2. Mount the test piece onto the aluminum test piece holder and screw into the back side of the water tank. Vaseline white petroleum jelly should be used to lubricate the threads
3. Place the water tank on a stable, horizontal surface
4. Place the pump and outlet tubing into a large container filled with water
5. Open the Insight PIV software on the computer
6. Align the PIV camera so that the desired test area is in focus
7. Align the laser sheet so that it illuminates the desired section of flow (slightly downstream across the middle of the cylinder). The lenses used for this experiment were, from top to bottom, -25, -15, and 1000 mm. The laser should be operated on a low-light setting during the alignment process. Be sure to wear eye protection whenever the laser is being used
8. Once all of the components of the experimental apparatus are aligned, the pump can be connected to a power source
9. Once the flow though the tank has stabilized data can be collected
10. Turn off the lights prior to activating the laser
11. Set the PIV software to capture the desired sequence of images, with the appropriate Q-switch delay and dt (time between images). It is also necessary to specify the pulse delay and pulse repetition, and to scale the image. The settings used for this experiment are listed below:

    sequence: 350 image pairs

    Q-switch delay: ranged between 150 – 160 μs

    dt: 700 μs

    pulse delay: 0.27 μs

pulse repetition rate: 15 Hz

scaling: 147.672 μm per pixel

12. Use TechPlot software to filter and analyze the images. Apply a three standard deviation filter on the data, twice
13. To switch test pieces, turn off the pump and drain the tank. Unscrew the mounting piece and replace the test piece. Rescrew the mounting piece into the tank wall and then reconnect the pump to the power source